Check for

#### RESEARCH ARTICLE SUMMARY

#### **IMMUNOLOGY**

### Germline mutations in a G protein identify signaling cross-talk in T cells

Hyoungjun Ham<sup>†</sup>, Huie Jing<sup>†</sup>, Ian T. Lamborn<sup>†</sup> et al.

**INTRODUCTION:** G protein-coupled receptors (GPCRs) direct cells to respond to diverse environmental cues including hormones, neurotransmitters, and chemokines. This is accomplished through a complex biochemical cycle mediated by associated heterotrimeric G proteins  $(G_{\alpha\beta\gamma})$ . After GPCR ligation, the  $G_{\alpha}$  subunit binds GTP, becomes active, and dissociates from both the  $G_{\beta\gamma}$  complex and GPCR. Dissociated  $G_{\alpha}$ -guanosine triphosphate (GTP) and free G<sub>By</sub> initiate downstream signals, including generation of second messengers, biochemical interactions, and ion fluxes. The GTPase activity of  $G_{\alpha}$  hydrolyzes GTP into guanosine diphosphate (GDP) to terminate signaling and allow reassembly of  $G_{\alpha\beta\gamma}$ with GPCR so that cells can respond to GPCR re-engagement. Among the  $G_{\alpha}$  proteins, the G<sub>0i/o</sub> family includes inhibitory isoforms that are thought to regulate biological responses by suppressing adenylyl cyclase (AC) production of cyclic adenosine monophosphate (cAMP). AC exists as transmembrane isoforms expressed broadly, with different tissues expressing different levels of multiple isoforms, but only certain ACs are sensitive to the inhibitory effects of G<sub>ci</sub>.  $G_{\alpha i2}$  (encoded by GNAI2) has been implicated in normal functioning of the cardiovascular, nervous, endocrine, and immune systems. However, the roles of Gai2 in human physiology and development, including the effect of germline GNAI2 mutations in humans, are not clear. Furthermore, how active  $G_{\alpha i/o}$  acts proximally through alternative mechanisms-not involving AC-mediated production of cAMP-to regulate downstream signal transduction is less well understood.

**RATIONALE:** Humans with monogenic inborn errors responsible for extreme disease phenotypes can reveal essential physiological pathways. We identified patients that harbored previously unreported or extremely rare GNAI2 mutations to examine their clinical presentations and their underlying disease mechanisms. In delineating molecular mechanisms underlying the mutations' prominent effects on the immune system, we tested the hypothesis that  $G_{\alpha i2}$  can regulate immune cell functions independently of cAMP.

**RESULTS:** We discovered 20 patients from 18 families with previously unreported or extremely rare heterozygous mutations in GNAI2 ( $G_{\alpha i2}$ ). The mutations were biochembinding, decreased GTP hydrolysis [in absence or presence of GTPase-activating protein (GAP)], and decreased cAMP production. The patients had multiorgan dysfunction, with a spectrum of birth defects involving brain, endocrine, skeletal, and other systems. Prominent immune dysregulation resulted from increased infection susceptibility-caused by impaired GPCR signaling for migration of T cells and neutrophils-and life-threatening autoimmunity with T cell hyperresponsiveness. We observed enhanced T cell receptor (TCR)-induced T cell activation and proliferation across varying stimulation conditions, along with enhanced distal regulatory S6 signaling. These effects occurred independently of AC-mediated cAMP production. Using quantitative proteomics, we identified RASA2, a GAP for RAS, among active G<sub>012</sub> interactors. Levels of T cell hyperactivation in RASA2 knockout patient T cells were comparable whether or not activated  $G_{\alpha i2}$  was also present, indicating that activated  $G_{\alpha i2}$  regulated these T cell responses completely or largely through RASA2. Activating G<sub>012</sub> proteins did not inhibit RASA2's GAP activity toward RAS but instead sequestered RASA2 toward the plasma membrane. This promoted RAS activation from the Golgi, thereby increasing downstream ERK/MAPK and PI3K-AKT S6 signaling to drive cellular growth and proliferation.

ically activating, as shown by increased

CONCLUSION: Humans with constitutively activating GNAI2 mutations show that Goi2 normally regulates diverse physiologic processes with major effects on the immune system. In studying their disease, we found enhanced suppression of effector cAMP generation and established a likely pathogenic role of chronic decoupling of active  $G_{\alpha i2}$  from GPCR for impaired leukocyte migration. We have unveiled a  $G_{\alpha i2}$ -mediated but cAMPindependent RAS-regulatory pathway that controls the amplification of T cell responses by intracellularly rerouting RASA2 away from RAS. Besides defining an inherited syndromic disorder within the RASopathy spectrum, our work identifies  $G_{\alpha i2}$  as a molecular linchpin immediately upstream of RASA2 at the nexus of GPCR and TCR signaling pathways. When activated, G<sub>012</sub> can potentially coordinate cell migration arrest with signals promoting T cell activation outcomes.

Normal T cells T cells with activating Patients with activating **G**<sub>ci2</sub> mutation G., mutation T cell infiltrates in **GPCR GPCR** lung, brain and liver Autoimmune hemolytic anemia **Psoriasis** mmunodysregulation Hashimoto thyroiditis Normal RAS activity **RAS** hyperactivation Autoimmune enteropathy/colitis Diabetes mellitus Normal T cell activation T cell hyperactivation No disease and hyperproliferation

Activated Gaiz bypasses cAMP to regulate human immunity. Constitutively activating GNAI2 mutations cause multiorgan dysfunction. Compared with normal T cells (left), T cells from patients signal through a cAMP-independent pathway involving  $G_{\alpha i2}$  (yellow), RASA2 (magenta), and RAS (green). This promotes antigen receptor-stimulated T cell hyperresponsiveness and autoimmunity. [Figure created with BioRender.com.]

The list of author affiliations is available in the full article online. \*Corresponding author: Helen C. Su (hsu@niaid.nih.gov) +These authors contributed equally to this work. Cite this article as H. Ham et al., Science 385, eadd8947 (2024). DOI: 10.1126/science.add8947



#### **READ THE FULL ARTICLE AT**

https://doi.org/10.1126/science.add8947

#### RESEARCH ARTICLE

#### **IMMUNOLOGY**

# Germline mutations in a G protein identify signaling cross-talk in T cells

Hyoungjun  $\operatorname{Ham}^{1,2,3}\dagger \ddagger$ , Huie  $\operatorname{Jing}^{1,2}\ddagger$ , Ian T. Lamborn $^{1,2,4}\ddagger$ , Megan M. Kober $^{1,2}\S$ , Alexey Koval $^5\S$ , Yamina A. Berchiche<sup>6</sup>§, D. Eric Anderson<sup>7</sup>, Kirk M. Druey<sup>8</sup>, Judith N. Mandl<sup>9</sup>¶, Bertrand Isidor<sup>10,11</sup>. Carlos R. Ferreira<sup>12</sup>, Alexandra F. Freeman<sup>13</sup>, Sundar Ganesan<sup>14</sup>, Meliha Karsak<sup>15,16</sup>, Peter J. Mustillo<sup>17,18</sup>, Juliana Teo<sup>19</sup>, Zarazuela Zolkipli-Cunningham<sup>20,21</sup>, Nicolas Chatron<sup>22,23</sup>, François Lecoquierre<sup>24</sup>, Andrew J. Oler<sup>25</sup>, Jana Pachlopnik Schmid<sup>26,27</sup>, Douglas B. Kuhns<sup>28</sup>, Xuehua Xu<sup>29</sup>, Fabian Hauck<sup>30</sup>, Waleed Al-Herz<sup>31,32</sup>, Matias Wagner<sup>33,34,35</sup>, Paulien A. Terhal<sup>36</sup> Mari Muurinen<sup>37,38,39</sup>, Vincent Barlogis<sup>40,41</sup>, Phillip Cruz<sup>25</sup>, Jeffrey Danielson<sup>1,2</sup>, Helen Stewart<sup>42</sup>, Petra Loid<sup>37,38,39</sup>, Sebastian Rading<sup>15,16</sup>, Boris Keren<sup>43,44</sup>, Rolph Pfundt<sup>45</sup>, Kol A. Zarember<sup>13</sup>, Katharina Vill<sup>46</sup>, Lorraine Potocki<sup>47,48</sup>, Kenneth N. Olivier<sup>49</sup>, Gaetan Lesca<sup>22,23</sup>, Laurence Faivre<sup>50,51</sup>, Melanie Wong<sup>52</sup>, Anne Puel<sup>53,54,55</sup>, Janet Chou<sup>56</sup>, Maud Tusseau<sup>57,58</sup>, Niki M. Moutsopoulos<sup>59</sup>, Helen F. Matthews<sup>2,60</sup>, Cas Simons<sup>61,62</sup>, Ryan J. Taft<sup>63,64</sup>, Ariane Soldatos<sup>65</sup>, Etienne Masle-Farquhar<sup>66,67</sup> Stefania Pittaluga<sup>68</sup>, Robert Brink<sup>69,70</sup>, Danielle L. Fink<sup>28</sup>, Heidi H. Kong<sup>71</sup>, Juraj Kabat<sup>14</sup>, Woo Sung Kim<sup>29</sup>, Tatjana Bierhals<sup>16</sup>, Kazuyuki Meguro<sup>1,2</sup>, Amy P. Hsu<sup>13</sup>, Jingwen Gu<sup>25</sup>, Jennifer Stoddard<sup>72</sup>, Benito Banos-Pinero<sup>73</sup>, Maria Slack<sup>74</sup>#, Giampaolo Trivellin<sup>75</sup>\*\*††, Benoît Mazel<sup>51,76</sup>, Maarja Soomann<sup>26</sup>, Samuel Li<sup>25</sup>, Val J. Watts<sup>77</sup>, Constantine A. Stratakis<sup>75</sup>‡‡§§¶¶, Maria F. Rodriguez-Quevedo³, Ange-Line Bruel<sup>50,78</sup>, Marita Lipsanen-Nyman<sup>38</sup>, Paul Saultier<sup>40,79</sup>, Rashmi Jain<sup>80</sup>, Daphne Lehalle<sup>81</sup>, Daniel Torres<sup>1,2</sup>, Kathleen E. Sullivan<sup>82</sup>, Sébastien Barbarot<sup>83</sup>, Axel Neu<sup>84</sup>, Yannis Duffourd<sup>50,78</sup>, Morgan Similuk<sup>85</sup>, Kirsty McWalter<sup>86</sup>, Pierre Blanc<sup>44</sup>, Stéphane Bézieau<sup>10,11</sup>, Tian Jin<sup>29</sup>, Raif S. Geha<sup>56</sup>, Jean-Laurent Casanova<sup>53,54,55,87,88</sup>, Outi M. Makitie<sup>37,38,39</sup>, Christian Kubisch<sup>16,89</sup> Patrick Edery<sup>22,90</sup>, John Christodoulou<sup>62,91,92</sup>, Ronald N. Germain<sup>9</sup>, Christopher C. Goodnow<sup>66,93</sup>, Thomas P. Sakmar<sup>6,94</sup>, Daniel D. Billadeau<sup>3</sup>, Sébastien Küry<sup>10,11</sup>##, Vladimir L. Katanaev<sup>5,95</sup>##, Yu Zhang<sup>1,2</sup>##, Michael J. Lenardo<sup>2,4,60</sup>, Helen C. Su<sup>1,2,4</sup>\*

Humans with monogenic inborn errors responsible for extreme disease phenotypes can reveal essential physiological pathways. We investigated germline mutations in GNAI2, which encodes  $G_{cii2}$ , a key component in heterotrimeric G protein signal transduction usually thought to regulate adenylyl cyclase–mediated cyclic adenosine monophosphate (cAMP) production. Patients with activating  $G_{cii2}$  mutations had clinical presentations that included impaired immunity. Mutant  $G_{cii2}$  impaired cell migration and augmented responses to T cell receptor (TCR) stimulation. We found that mutant  $G_{cii2}$  influenced TCR signaling by sequestering the guanosine triphosphatase (GTPase)–activating protein RASA2, thereby promoting RAS activation and increasing downstream extracellular signal–regulated kinase (ERK)/mitogen-activated protein kinase (MAPK) and phosphatidylinositol 3-kinase (PI3K)–AKT S6 signaling to drive cellular growth and proliferation.

protein-coupled receptors (GPCRs) are fundamental to mammalian physiology (1,2). They direct cells to respond to diverse environmental cues, including hormones, neurotransmitters, and chemokines. This is accomplished through a complex, highly regulated biochemical cycle mediated by associated heterotrimeric G proteins ( $G_{\alpha\beta\gamma}$ ). After GPCR ligation, the  $G_{\alpha}$  subunit binds guanosine triphosphate (GTP), becomes active, and dissociates from both the  $G_{\beta\gamma}$  complex and the GPCR. Dissociation causes both  $G_{\alpha}$ -GTP and free  $G_{\beta\gamma}$  to initiate downstream signals, including generation of second messengers and ion fluxes. Ultimately, the GTPase activity of  $G_{\alpha}$  hydrolyzes GTP into guanosine diphosphate (GDP) to terminate signaling and allow reassembly of the heterotrimeric G protein that can reassociate with a GPCR, completing the cycle and resetting cells to allow them to respond again to GPCR engagement (3).

The 16 human  $G_{\alpha}$  subunits are grouped into four families ( $G_{\alpha s}$ ,  $G_{\alpha i/o}$ ,  $G_{\alpha q/11}$ , and  $G_{\alpha 12/13}$ ) having distinct expression patterns and effector partners (4). The  $G_{\alpha i/o}$  family includes inhibitory isoforms of  $G_{\alpha}$  that are thought to regulate biological responses by suppressing adenylyl cyclase (AC) production of the intracellular second messenger cyclic adenosine monophosphate (cAMP) (5). AC exists as nine transmembrane isoforms expressed broadly, with different tissues expressing different levels of multiple isoforms (6, 7). Only group III (AC5 and AC6) and to a lesser degree group I (AC1) ACs are sensitive to the inhibitory effects of  $G_{\alpha i}$  (6, 7).

Humans with monogenic inborn errors responsible for extreme disease phenotypes can reveal essential physiological pathways. Germline mutations in  $G_{\rm cijo}$  family members (GNAII, GNAI3, GNAOI, GNAT1, and GNAT2) cause severe neurodevelopmental, craniofacial, or visual system defects (8–10). By contrast, the effect

of germline GNAI2 mutations in humans is not known. Although  $G_{ci2}$  (encoded by GNAI2) is ubiquitously expressed, it has been implicated in normal functioning of the cardiovascular, nervous, endocrine, and immune systems (11, 12). Somatic GNAI2 mutations that activate  $G_{ci2}$  have been identified in human ovarian and adrenal tumors (13). GNAI2 variants of uncertain significance were also identified in two individuals with neurodevelopmental defects (14, 15).

Because the roles of  $G_{\rm ci2}$  in human physiology and development are not clear, we sought to identify individuals that harbor mutations in GNAI2 to examine their clinical presentations and their underlying disease mechanisms.

# **GNAI2** mutations found in humans inhibited the intrinsic GTPase activity

We used whole-exome and whole-genome sequencing to discover 20 patients from 18 unrelated families of different ancestries worldwide, who had previously unreported or extremely rare heterozygous missense variants in GNAI2, which were also computationally predicted to be deleterious [combined annotation-dependent depletion (CADD) score >25] (Fig. 1A and table S1). The variants were absent in the Greater Middle Eastern Variome (16) and in the Genome Aggregation Database (gnomAD v3.1.2) (17), except for 3-50256263-G-A (GRCh38, p. Arg179His), which was found in one individual [minor allele frequency (MAF) 0.00002494 in the African and African American population] of unknown affectation status. In our families, the variants segregated with a hitherto unrecognized autosomal dominant syndromic disorder, in which de novo (n = 12) mutations predominated. These mutations were detected in several tissues (fig. S1, A and B), suggesting that they arose in germ cells or early during embryonic development. The patients' cells expressed equivalent levels of both mutant and wild-type (WT) transcripts, as well as normal levels of total  $G_{\alpha i2}$  protein (fig. S1, C and D).

The mutations caused amino acid substitutions at residues that were evolutionarily constrained and highly conserved in all heterotrimeric G protein superfamily members (Fig. 1B and fig. S1E). The altered residues were clustered in the Ras-like GTPase domain of  $G_{\alpha}$ , especially within the highly conserved P-loop motif and switch regions that are critical for guanine-nucleotide binding and GTPase activity (Fig. 1B and fig. S1E). These mutations could interfere with binding of the GTP phosphate group and cofactors (Mg<sup>2+</sup> ion and nucleophilic H<sub>2</sub>O) that are necessary to hydrolyze bound GTP (Fig. 1 C) or could indirectly influence GTP binding and hydrolysis (fig. S2, A to C), which would likely result in impaired signal termination (see supplementary text 1).

We tested the function of purified recombinant  $G_{\alpha i2}$  variant proteins and compared their ability to bind and hydrolyze GTP with nonmutated WT  $G_{\alpha i2}$  and a GTPase mutant

(Gln<sup>205</sup>→Leu) known to be deficient in GTP hydrolysis (18). In general, the  $G_{\alpha i2}$  mutants, except Arg<sup>179</sup>→His, bound nonhydrolyzable  $GTP_{\gamma}S$  (a GTP analog that locks  $G_{\alpha i2}$  in an active state) more readily than WT (Fig. 1, D and E; fig. S2, D to F; and table S2), and all exhibited decreased GTP hydrolysis (Fig. 1, F and G; fig. S2, G to J; and table S2).

To substantiate the conclusion that the mutations in Gai2 impaired GTPase activity, we investigated their regulation by regulators of G protein signaling (RGS). The intrinsic GTPase activity of G<sub>oi</sub> is normally accelerated by RGS,

which act as GTPase-activating proteins (GAPs) and are strictly dependent on binding to a  $G_{\alpha}$  transition-state conformation (18). GTPasedeficient  $G_{\alpha}$  mutants, such as  $G_{\alpha il}$ - $Gln^{204}$  $\rightarrow$ Leu, are generally resistant to RGS GAP activity (19). Accordingly, the GTPase activities of the patients' G<sub>ci2</sub> mutants, except Arg<sup>179</sup>→His, were not increased by adding RGS16 (Fig. 1G and fig. S2J). Furthermore, neither of two patient mutants that we tested (Thr $^{182}$  $\rightarrow$ Ala/ $\rightarrow$ Ile nor Gln<sup>205</sup>→Leu) bound RGS16 (fig. S2, K and L), which is similar to what was observed with an RGS-insensitive Gly<sup>184</sup>→Ser control (20). Taken together, the faster GTP binding, decreased GTPase activity, and RGS insensitivity indicated that the patients'  $G_{\alpha i2}$  mutant proteins could promote a GTP-bound form of  $G_{\alpha i2}$ , in this way delaying signal termination and prolonging  $G_{\alpha i2}$  activity (table S2).

This constitutive activation of G<sub>0i2</sub> would be expected to overstimulate downstream functions such as inhibition of cAMP production (5). Therefore, we measured forskolin (FSK)-induced AC synthesis of cAMP in the presence of overexpressed  $G_{\alpha i2}$ . Compared with WT, mutant  $G_{\alpha i2}$ found in patients suppressed accumulated cAMP

1-Human Immunological Diseases Section, Laboratory of Clinical Immunology and Microbiology, Division of Intramural Research (DIR), National Institute of Allergy and Infectious Diseases (NIAID), National Institutes of Health (NIH), Bethesda, MD, USA. <sup>2</sup>Clinical Genomics Program, DIR, NIAID, NIH, Bethesda, MD, USA. <sup>3</sup>Division of Oncology Research, Schulze Center for Novel Therapeutics, Mayo Clinic, Rochester, MN, USA. <sup>4</sup>Department of Pathology and Laboratory Medicine, Perelman School of Medicine, University of Pennsylvania, Philadelphia, PA, USA. <sup>5</sup>Department of Cell Physiology and Metabolism, Faculty of Medicine, Translational Research Center in Oncohaematology, University of Geneva, Geneva, Switzerland. Elaboratory of Chemical Biology and Signal Transduction, The Rockefeller University, New York, NY, USA. Advanced Mass Spectrometry Facility, National Institute of Diabetes and Digestive and Kidney Diseases (NIDDK), NIH, Bethesda, MD, USA. Lung and Vascular Inflammation Section Laboratory of Allergic Diseases, DIR, NIAID, NIH, Bethesda, MD, USA. 9Lymphocyte Biology Section, Laboratory of Immune System Biology, DIR, NIAID, NIH, Bethesda, MD, USA. 10 Service de Génétique Médicale, CHU Nantes, Nantes Université, Nantes, France. 11 L'Institut du Thorax, CHU Nantes, INSERM UMR 1087/CNRS UMR 6291, Nantes Université, Nantes, France. 12 Skeletal Genomics Unit, Metabolic Medicine Branch, DIR, National Human Genome Research Institute (NHGRI), NIH, Bethesda, MD, USA. <sup>13</sup>Laboratory of Clinical Immunology and Microbiology, DIR, NIAID, NIH, Bethesda, MD, USA. <sup>14</sup>Biological Imaging Section, Research Technologies Branch, DIR, NIAID, NIH, Bethesda, MD 20892, USA. <sup>15</sup>Neuronal and Cellular Signal Transduction, Center for Molecular Neurobiology Hamburg (ZMNH), University Medical Center Hamburg-Eppendorf, Hamburg, Germany, <sup>15</sup>Institute of Human Genetics, University Medical Center Hamburg-Eppendorf, Hambu <sup>20</sup>Mitochondrial Medicine Frontier Program, Division of Human Genetics, Department of Pediatrics, Children's Hospital of Philadelphia, Philadelphia, PA, USA. <sup>21</sup>Department of Pediatrics, University of Pennsylvania Perelman School of Medicine, Philadelphia, PA, USA. 22 Service de Génétique, Hospices Civils de Lyon, Lyon, France. 23 Institut NeuroMyoGène, Physiopathologie et Génétique du Neurone et du Muscle, CNRS UMR 5261, INSERM UJ315, Université Claude Bernard Lyon 1, Lyon, France. <sup>24</sup>Université de Rouen Normandie, INSERM UJ2045 and CHU Rouen, Department of Genetics and Reference Center for Developmental Disorders, FHU-G4 Génomique, Rouen, France. <sup>25</sup>Bioinformatics and Computational Biosciences Branch, Office of Cyber Infrastructure and Computational Biology (OCICB), NIAID, NIH, Bethesda, MD, USA. <sup>26</sup>Division of Immunology, University Children's Hospital Zurich, Zurich, Switzerland. <sup>27</sup>Pediatric Immunology, University of Zurich, Zurich, Switzerland. <sup>28</sup>Neutrophil Monitoring Lab, Applied/Developmental Research Directorate, Frederick National Laboratory for Cancer Research, Frederick, MD, USA. <sup>29</sup>Chemotaxis Signal Section, Laboratory of Immunogenetics, DIR, NIAID, NIH, Rockville, MD, USA. 30 Division of Pediatric Immunology and Rheumatology, Department of Pediatrics, Dr. von Hauner Children's Hospital, University Hospital, Ludwig-Maximilians-Universität (LMU), Munich, Germany. <sup>31</sup>Department of Pediatrics, Faculty of Medicine, Kuwait University, Kuwait City, Kuwait <sup>32</sup>Department of Pediatrics, Al-Sabah Hospital, Kuwait City, Kuwait University Munich, School of Medicine and Health, Munich, Germany. <sup>34</sup>Institute of Neurogenomics, Helmholtz Zentrum München, Neuherberg, Germany. <sup>35</sup>Department of Pediatrics, Division of Pediatric Neurology, Developmental Medicine and Social Pediatrics, University Hospital of Munich, Munich, Germany, <sup>36</sup>Division of Laboratories, Pharmacy and Biomedical Genetics, University Medical Centre Utrecht, Utrecht, The Netherlands. <sup>37</sup>Folkhälsan Research Center, Genetics Research Program, Helsinki, Finland. <sup>38</sup>Children's Hospital, University of Helsinki and Helsinki University Hospital, Helsinki, Finland. <sup>39</sup>Research Program for Clinical and Molecular Metabolism, University of Helsinki, Finland. <sup>40</sup>APHM, La Timone Children's Hospital, Department of Pediatric Hematology, Immunology, and Oncology, Marseille, France. 41 Aix-Marseille University, EA 3279 Research Unit, Marseille, France. 42 Oxford Centre for Genomic Medicine, Nuffield Orthopaedic Centre, Oxford University Hospitals, NHS Foundation Trust, Headington, Oxford, UK. <sup>43</sup>Genetic Departement, Assistance Publique - Hôpitaux de Paris Sorbonne University, Paris, France. <sup>44</sup>SeqOlA Laboratory, FMG2025, Paris, France. <sup>45</sup>Department of Human Genetics, Donders Institute for Brain, Cognition and Behaviour, Radboud University Medical Center, Nijmegen, Netherlands. 46LMU University Hospital, Department of Pediatrics, Division of Pediatric Neurology, iSPZ Hauner MUC - Munich University Center for Children with Medical and Developmental Complexity, Dr. von Hauner Children's Hospital, Munich, Germany. 47Department of Molecular and Human Genetics, Baylor College of Medicine, Houston, TX, USA. <sup>48</sup>Texas Children's Hospital, Houston, TX, USA. <sup>49</sup>Pulmonary Branch, Division of Intramural Research, DIR, National Heart Lung and Blood Institute (NHLBI), NIH, Bethesda, MD, USA. <sup>50</sup>Génétique des Anomalies du Développement (GAD), UMR 1231, INSERM, Université Bourgogne-Franche Comté, Dijon, France. <sup>51</sup>Centre de Génétique et Centre de Référence "Anomalies du Développement et Syndromes Malformatifs de l'Inter-région Est", FHU TRANSLAD, CHU Dijon Bourgogne, Dijon, France. <sup>52</sup>Department of <sup>31</sup>Centre de Génétique et Centre de Référence "Anomalies du Développement et Syndromes Maltormatits de l'Inter-région LSt."; FHU I HANSLAU, CHU Dijon Bourgogne, Dijon, France. "Department or Allergy and Immunology, The Children's Hospital at Westmead, Sydney, NSW, Australia. <sup>53</sup>St. Giles Laboratory of Human Genetics of Infectious Diseases, Rockefeller Branch, The Rockefeller University, New York, NY, USA. <sup>54</sup>Laboratory of Human Genetics of Infectious Diseases, Necker Branch, Institut National de la Santé et de la Recherche Médicale, INSERM U1163, Paris, France. <sup>56</sup>Inision of Immunology, Boston Children's Hospital, Department of Pediatrics, Harvard Medical School, Boston, MA, United States. <sup>57</sup>Genetics Department, Lyon University Hospital, Lyon, France. <sup>58</sup>The International Center of Research in Infectiology, Lyon University, INSERM U1111, CNRS UMR 5308, ENS, UCBL, Lyon, France. <sup>59</sup>Oral Immunity and Infection Section, DIR, National Institute of Dental and Craniofacial Research (NIDCR), NIH, Bethesda, MD, USA. <sup>60</sup>Molecular Development of the Immune System Section, Laboratory of Immune System Biology, DIR, NIAID, NIH, Bethesda, MD, USA. <sup>61</sup>Centre for Population Genomics, Garvan Institute of Medical Research and UNSW Sydney, Sydney, Sydney, NSW, Australia. <sup>62</sup>Murdoch Children's Research Institute, Melbourne, Victoria, Australia. <sup>63</sup>Institute for Molecular Bioscience, University of Queensland, St. Lucia, Queensland, Australia. <sup>64</sup>Illumina, San Diego, CA, USA. <sup>65</sup>National Institute of Neurological Discorders and Stroke (NINDS). NIH, Bethesda, MD, USA. <sup>66</sup>Immunogenomics Laboratory, Garvan Institute of Medical Research. Sydney, NSW, Australia. <sup>67</sup>School of Clinical Medicine LINSW Sydney. Disorders and Stroke (NINDS), NIH, Bethesda, MD, USA. 66 Immunogenomics Laboratory, Garvan Institute of Medical Research, Sydney, NSW, Australia. 67 School of Clinical Medicine, UNSW Sydney, Sydney, NSW, Australia. 68 Laboratory of Pathology, Center for Cancer Research, NCI, NIH, Bethesda, MD, USA. 69 St. Vincent's Clinical School, UNSW, Sydney, NSW, Australia. 70 B Cell Biology Laboratory, Garvan Institute of Medical Research, Sydney, NSW, Australia. <sup>71</sup>Cutaneous Microbiome and Inflammation Section, Dermatology Branch, National Institute of Arthritis and Musculoskeletal and Skin Diseases (NIAMS), NIH, Bethesda, MD, USA. <sup>72</sup>Immunology Service, Department of Laboratory Medicine, Clinical Center, NIH, Bethesda, MD, USA. <sup>73</sup>Oxford Genetics Laboratories, Oxford University Hospitals NHS Foundation Trust, Oxford, Oxfordshire, UK. <sup>74</sup>Division of Allergy and Immunology, Department of Pediatrics, University of Rochester Medical Center and Golisano Children's Hospital, Rochester, NY, USA. <sup>75</sup>Section on Endocrinology and Genetics (SEGEN), DIR, *Eunice Kennedy Shriver* National Institute of Child Health and Human Development (NICHD), NIH, Bethesda, MD, USA. <sup>76</sup>Centre de Référence Déficiences Intellectuelles de Causes Rares, CHU Dijon Bourgogne, Dijon, France. <sup>77</sup>Department of Medicinal Chemistry and Molecular Pharmacology, Purdue University, West Lafayette, IN, USA. <sup>78</sup>Unité Fonctionnelle Innovation en Diagnostic Génomique des Maladies Rares, FHU TRANSLAD, CHU Dijon Bourgogne, Dijon, France. <sup>79</sup>Aix-Marseille University, INSERM, National Research Institute for Agriculture, Food and Environment (INRAe), Cardiovascular and Nutrition Research Center (C2VN), Marseille, France. <sup>80</sup>Clinical Immunology, Oxford University Hospitals NHS Foundation Trust, Oxford, UK. 81AP-HP Sorbonne Université, UF de Génétique Clinique, Centre de Référence Maladies Rares des Anomalies du Développement et Syndromes Malformatifs, Hôpital Trousseau, Paris, France. <sup>82</sup>Division of Allergy and Immunology, Children's Hospital of Philadelphia, Ph., USA. <sup>83</sup>Department of Dermatology, CHU Nantes, INRAE, UMR 1280, PhAN, Nantes Université, Nantes, France. <sup>84</sup>Department of Pediatrics, University Medical Center Hamburg-Eppendorf, Hamburg, Germany. <sup>85</sup>Centralized Sequencing Program, DIR, NIAID, NIH, Bethesda, MD, USA. <sup>86</sup>GeneDx, Gaithersburg, MD, USA. <sup>87</sup>Howard Hughes Medical Institute, New York, NY, USA. <sup>88</sup>Department of Pediatrics, Necker Hospital for Sick Children, Paris, France. <sup>89</sup>Martin Zeitz Center for Rare Diseases, University Medical Center Hamburg-Eppendorf, Hamburg, Germany. 90 Centre de Recherche en Neurosciences de Lyon, Inserm U1028, UMR CNRS 5292, Université Claude Bernard Lyon 1, Lyon, France. 91 Department of Paediatrics, University of Melbourne, Melbourne, Australia. 92 Specialty of Child and Adolescent Health, University of Sydney, Sydney, Australia.

#### \*Corresponding author. Email: hsu@niaid.nih.gov

†Present address: Division of Oncology Research, Schulze Center for Novel Therapeutics, Mayo Clinic, Rochester, MN, USA.

<sup>‡</sup>These authors contributed equally to this work.

These authors contributed equally to this work.

<sup>¶</sup>Present address: Department of Physiology, McGill University, Montreal, QC Canada.

<sup>#</sup>Present address: Blanchard Valley Hospital, Findlay, OH, USA.

<sup>\*\*</sup>Present address: Department of Biomedical Sciences, Humanitas University, Milan, Italy.

<sup>††</sup>Present address: IRCCS Humanitas Research Hospital, Milan, Italy.

<sup>‡‡</sup>Present address: IMMB, FORTH, Heraklion, Crete, Greece.

<sup>§§</sup>Human Longevity, San Diego, CA, USA,

<sup>¶¶</sup>StereoTherapeutics, Doylestown, PA, USA.

<sup>##</sup>These authors contributed equally to this work.

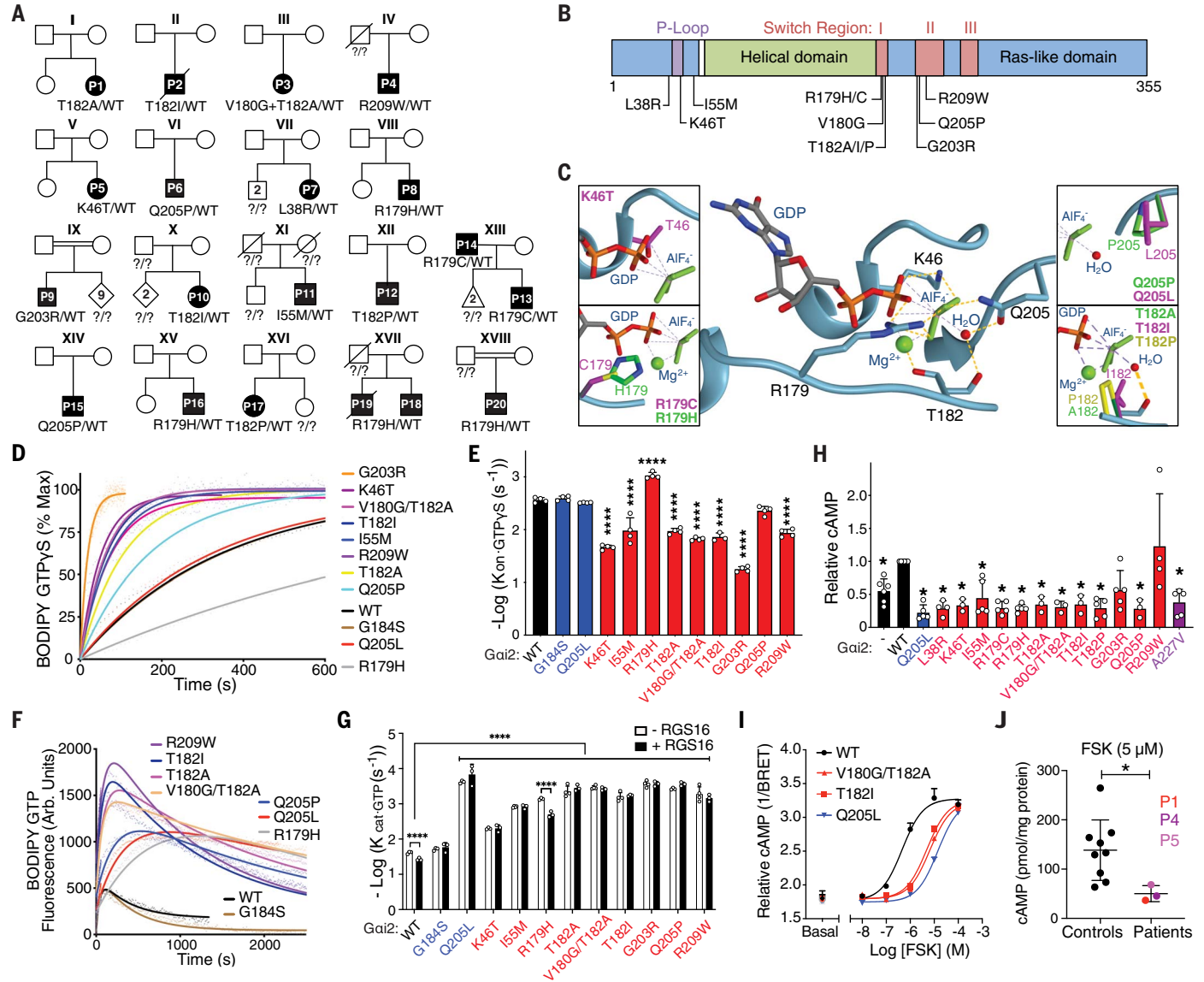


Fig. 1. Humans with biochemically activating GNAI2 mutations. (A) Patient pedigrees showing mutations and affected status. P8 was previously reported in a large cohort of individuals with developmental disorders (14). Single-letter abbreviations for the amino acid residues are as follows: A, Ala; C, Cys; G, Gly; H, His; I, Ile; K, Lys; L, Leu; M, Met; P, Pro; Q, Gln; R, Arg; S, Ser; T, Thr; V, Val; W, Trp; and Y, Tyr. (**B**) Location of mutations in the  $G_{\alpha i2}$  protein, numbered according to the longest isoform that predominates across tissues including blood. (**C**) Structural model of  $G_{\alpha i2} \cdot GDP \cdot Mg^{2+} \cdot AlF4^-$ , showing interactions in the GTPase catalytic site.  $AlF_4^-$  is a  $\gamma$ -phosphate mimic that acts as a transition-state analog. Dashed lines indicate noncovalent bonds. Yellow dashed lines indicate those mediated by G<sub>ci2</sub>. (Insets) Patient variants are shown disrupting the interactions. The noncovalent bond between amino acid 182 and the nucleophilic H<sub>2</sub>O is with the backbone amide oxygen on the residue. PDB: 1GFI. (**D**) GTP binding of nonhydrolyzable GTP<sub> $\nu$ </sub>S by purified recombinant  $G_{\alpha i2}$  proteins. (**E**) Binding rate constants ( $k_{on \cdot GTP_YS}$ ) from (D). Red indicates patient variants. Blue indicates  $Q^{205}\rightarrow L$ , which is a GTPase-deficient positive control (18), and  $G^{184} \rightarrow S$ , which is an RGS-insensitive control (normal GDP/GTP exchange and intrinsic GTPase activity but impaired RGS-mediated GTPase activity) (20). (**F**) GTPase assay. (**G**) Hydrolysis rate constants ( $k_{cat \cdot GTP}$ ), with (black) or without

(white) RGS16, from (F). (H) FSK-stimulated cAMP in 293T cells after transfection with  $G_{\alpha i2}$  variants, measured by ELISA. The increased cAMP in WTtransfected as compared to untransfected cells may reflect heterologous sensitization of AC (76). Purple, A<sup>227</sup> → V, variant of uncertain significance (15). (I) FSK-stimulated cAMP reporter activity in HEK293 cells transfected with G<sub>cri2</sub> variants and YFP-EPAC-RLuc reporter (and CXCR4). Relative cAMP was expressed as 1/BRET. YFP, yellow fluorescent protein. (J) cAMP accumulation in primary fibroblasts from patients or healthy donors after FSK stimulation (basal levels provided in fig. S3I). Data show representative experiments [(D), (F), and (I)] or mean ± SD [(E), (G), (H), and (J)] for three to five independent experiments [(D) to (I)] or for three patients (J). Individual points within graphs represent results from independent experiments [(E), (G), (H), and (J)]. Statistical analyses were performed using one-way analysis of variance (ANOVA) with Tukey's multiple comparisons test for comparing individual variants with WT for (E) and (G) [for (G), without RGS]; multiple t tests using the Holm-Sidak method for comparison between GTP hydrolysis of  $G_{\alpha i2}$  protein with or without RGS16 for each variant [for (G), white versus black]; one-sample t test with twostage step-up method of Benjamini, Krieger, and Yekutieli with hypothetical value of 1 for (H); and unpaired t test for (J). \*P < 0.05; \*\*\*\*P < 0.0001.

production (Fig. 1H and fig. S3, A to D) or transient cAMP activity (Fig. 1I; fig. S3, E to H; and table S3). AC5 is a well-documented target of active  $G_{\alpha i2}$  inhibition (5), and we observed similar effects of mutant  $G_{\alpha i2}$  on AC5-induced cAMP production (fig. S3D). Lastly, primary dermal fibroblasts isolated from several patients (bearing Thr 182 → Ala, Lys 46 → Thr, and Arg<sup>209</sup>→Trp mutations) showed decreased cAMP production (Fig. 1J). However, two of the mutants that we tested, including Arg<sup>209</sup> → Trp, did not decrease cAMP production in the overexpression system (Fig. 1H and table S2). Mutations at Arg<sup>209</sup>, which is part of a highly conserved "Gly-Arg-Glu" triad found in all Ga family members, can disable G<sub>a</sub> activation of effectors because of the mutants' inability to dissociate from  $G_{B\nu}$  even in the GTP-bound conformation (supplementary text 2) (21).

Overall, our data suggested that the mutations in GNAI2 that we identified in patients impaired the GTPase activity of  $G_{\alpha i2}$  and enhanced the suppression of cAMP production, which would be consistent with them being pathogenic "activating" variants.

### Patients with GNAI2 mutations exhibited multiple clinical presentations

We next investigated the overall pathophysiological impact of the activating G<sub>012</sub> mutations by in-depth clinical phenotyping (data S1 and supplementary text 3 and 4). The patients exhibited abnormal development characterized by intrauterine growth retardation, dysmorphism (Fig. 2A), bone dysostosis (Fig. 2B), neuroanatomical abnormalities (Fig. 2C), and birth defects in other organs (Fig. 2D). Midline structural defects, located along the body's central vertical axis and suggestive of abnormal development during blastogenesis, were observed (fig. S4A). These were most commonly congenital nasal septum deviation (Fig. 2B), dysgenesis of the corpus callosum (Fig. 2C), pituitary hypoplasia with growth hormone deficiency (Fig. 2C), Chiari I malformation (Fig. 2C), micropenis, sagittal cleft ("butterfly") vertebrae (Fig. 2B), and scoliosis (Fig. 2B). The occurrence of certain rare birth defects, such as subcortical band heterotopia (Fig. 2C), agenesis of olfactory bulbs (Fig. 2C), and coloboma, suggested defective neuronal migration during late embryogenesis and early fetal development, including that of olfactory and gonadotropinreleasing hormone neurons as well as retinal progenitor cells. Most patients exhibited postnatal abnormalities too, including short stature with neurodevelopmental delay, neurobehavioral deficits, and gastrointestinal dysfunction (data S1 and supplementary text 3 and 4).

Weighted analysis of clinical features affected in each patient revealed heterogeneity in the systems affected across the cohort (Fig. 2E). Nearly all patients (90%) had disease involvement in the immune system, characterized by recurrent, unusual, and/or severe infections (data SI and supplementary text 3). However, the extent of disease involvement in the immune system was greater in patients mutated at residue Thr<sup>182</sup> owing to their additional inflammatory or autoimmune complications (Fig. 2E). An attempt to knock in the highly constitutively activating Thr<sup>182</sup>—Ile mutation into mice failed to generate heterozygous embryos beyond the eight-cell stage, indicating in utero lethality (table S4).

Among the immune system presentations (data S1 and supplementary text 3), bacterial, superficial fungal, or unusually severe viral infections of the skin were striking and included recurrent shingles, extensive warts, and rubella vaccine-associated skin granulomas (Fig. 2D and fig. S4, B and C). Respiratory, middle ear, and sinus infections were common with some developing bronchiectasis, and some had invasive bacterial infections (Fig. 2, B and D, and fig. S4, B and C). Inflammatory or autoimmune complications included lymphocytic infiltration of organs, psoriasis, discoid lupus, autoimmune cytopenias with splenomegaly, Hashimoto thyroiditis, type I diabetes mellitus, colitis, or macrophage activation syndrome (Fig. 2D and fig. S4). Several had asthma or atopic dermatitis (fig. S4). Longitudinal laboratory testing revealed monocytosis and neutrophilia precipitated by acute infection, which persisted in some patients (fig. S5A and supplementary text 5). T cell counts were initially low, with decreased recent thymic emigrants and paucity of naïve versus effector and memory T cells, but counts increased with age (fig. S5, B to D). Effector phenotype T cells showed cytokine perturbations, including increased interleukin-17 (IL-17) expression (fig. S5E). Lymphocyte proliferation and activation appeared normal or even increased (fig. S6 and table S5). Dysgammaglobulinemia, characterized by low serum immunoglobulin M and poorer vaccine titers, was accompanied by decreased B cell counts and atretic lymphoid follicles in secondary lymphoid organs (fig. S5, F and G; fig. S7; table S6; and supplementary text 6).

Overall, the patients' phenotypes indicated that mutant  $G_{vi2}$  caused multiorgan dysfunction, including life-threatening immunodysregulation and numerous birth defects. Their presentations underscore the importance of  $G_{vi2}$  in regulating diverse physiologic processes in humans.

## $G_{\alpha i2}$ mutant proteins impaired immune cell migration

The patients' clinical features suggested impaired migratory behavior of immune cells for host defense, which are guided to sites of infection by chemokine receptors. Because heterotrimeric G proteins transduce signals for all chemokine receptors (22), we tested whether hyperactive  $G_{\rm ci2}$  altered cell migration. Both CD4 $^+$  and CD8 $^+$  T cells from several patients showed decreased chemotaxis toward multi-

ple chemokines (Fig. 3A and fig. S8, A to D) and reduced chemokine-induced Ca<sup>2+</sup> fluxes mediated by free  $G_{\beta\gamma}$  subunits in one tested patient (Fig. 3B and fig. S8E), indicating defective proximal GPCR signaling. These defects were recapitulated by expressing all hyperactive  $G_{\alpha i2}$  mutant proteins except  $Ile^{55} \rightarrow Met$  in T cells from normal healthy donors, with intermediate and more variable effects of Leu<sup>38</sup>→Arg and Arg<sup>179</sup>→Cys (Fig. 3, C to E, and figs. S8, F to H, and S9, A to E). Neutrophils from several patients also showed reduced directional migration in response to chemoattractants (fig. S10, A and B), and their defective migration was recapitulated by expressing several hyperactive G<sub>ci2</sub> mutant proteins in the neutrophil-like HL60 cell line (fig. S10, C to F, and movies S1 to S3). These data would be consistent with immune cells having altered trafficking in patients with GNAI2 mutations. Indeed, in one patient with periodontitis, leukocytes had impaired accumulation in the oral mucosa or impaired migration into blisters after induction of sterile inflammation in the skin (fig. S10, G and H).

Furthermore, in two patients, splenic biopsies showed increased leukocyte numbers in red pulp with decreased white pulp (fig. S7 and supplementary text 6), suggesting that leukocyte migration into secondary lymphoid organs was also impaired. Hence, we tracked T cell migration in mice after adoptive transfer and found that cells expressing mutant  $G_{\alpha i2}$  proteins migrated less well into lymph nodes and splenic white pulp (Fig. 3F and fig. S9F). This might alter cell-cell interactions that normally take place within secondary lymphoid organs for developing immune cell functions.

Moreover, although suppressed cAMP could contribute to the impaired migration phenotype, the literature is contradictory (23). At least in T cells and neutrophils, pharmacologic manipulations that increase intracellular cAMP have been shown to inhibit chemotaxis (24, 25). Thus, we examined whether cAMP levels affected by Gqi2 mutants impact T cell chemotaxis. We used CRISPR-Cas9-mediated gene editing to knock out ADCYs encoding major ACs expressed in human T cells (fig. S11, A and B). Ablation of AC3 or AC7 in healthy donor T cells had opposite effects on endogenous cAMP levels but did not affect chemotaxis, which instead segregated with the absence or presence of the mutant  $G_{ci2}$  (Fig. 3, G to I, and fig. S11, C to G). These results suggested that the impaired leukocyte chemotaxis in the patients did not result from  $G_{\alpha i2}$ -mediated alterations in cAMP production.

Collectively, these findings showed that the patients' G<sub>ci2</sub> mutants caused defective cell migration. We hypothesized that the patients' mutants, being in a "quasipermanent" GTP-bound state of biochemical activation, might be mostly dissociated from GPCRs and therefore unable to transduce GPCR signals.

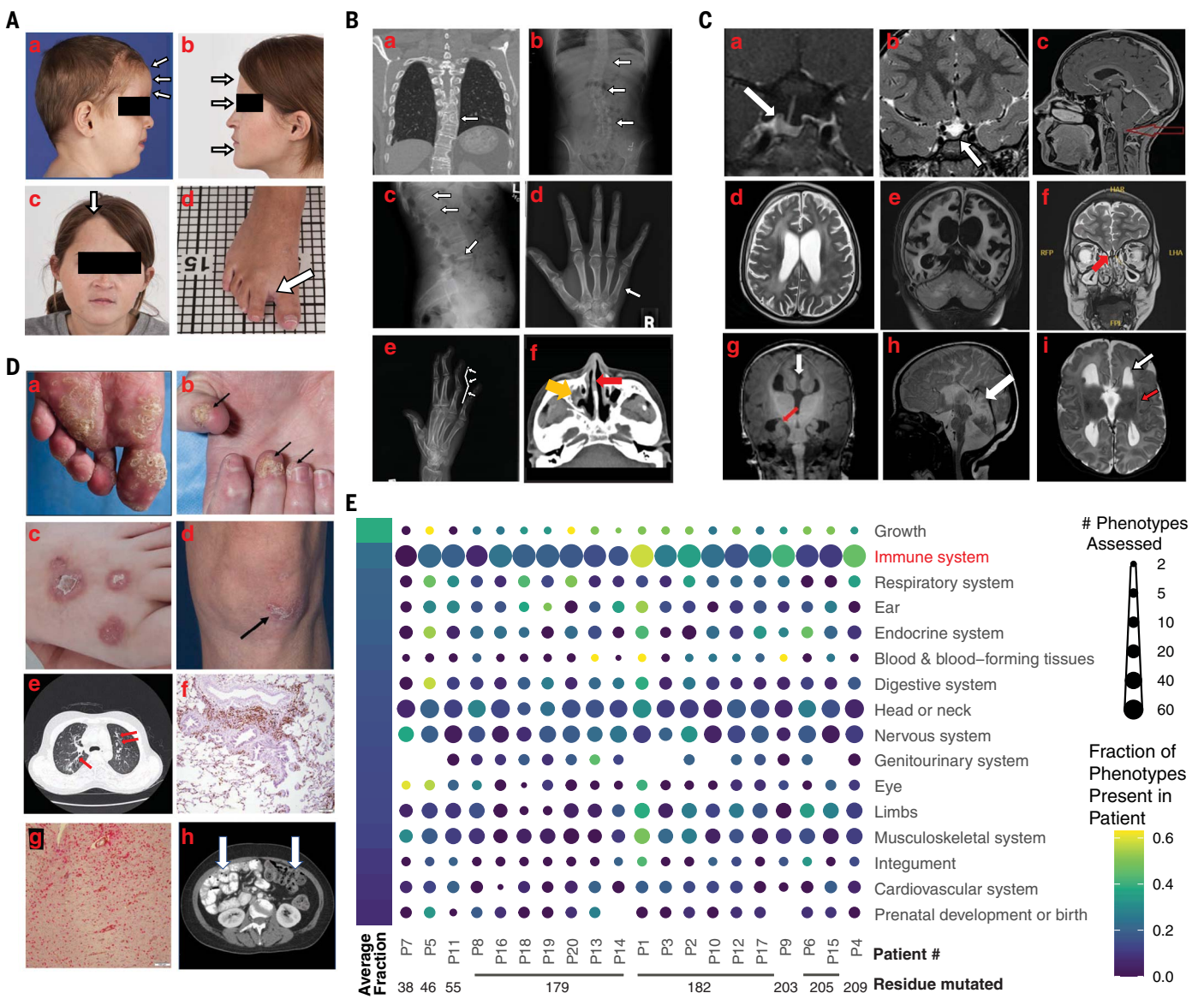


Fig. 2. Selected clinical features of patients with activating GNAI2 mutations. (A) Dysmorphism: frontal prominence (a), flat face (b), high anterior hairline (c), sandal gap deformity (d). (B) Skeletal abnormalities: sagittal cleft vertebra (a), scoliosis (b), irregular vertebral endplates (c), brachydactyly type E (d), swan-neck deformity (e), deviated nasal septum (red arrow) with chronic sinusitis (yellow arrow) (f). (C) Neurological and associated midline defects: misshapen sella turcica (a), hypoplastic pituitary gland (b), Chiari I malformation (c), diffuse leukodystrophy (d) progressing to end-stage neuro-degeneration (e), absence of olfactory bulbs (arrow shown for one side) (f), agenesis of the corpus callosum (white arrow) and hippocampus malrotation (red arrow) (g), cerebellar dysplasia (h), and polymicrogyria as well as subependymal (white arrow) and band (red arrow) heterotopia (i). (D) Infectious and inflammatory complications: persistent warts [(a) and (b)], rubella vaccine—

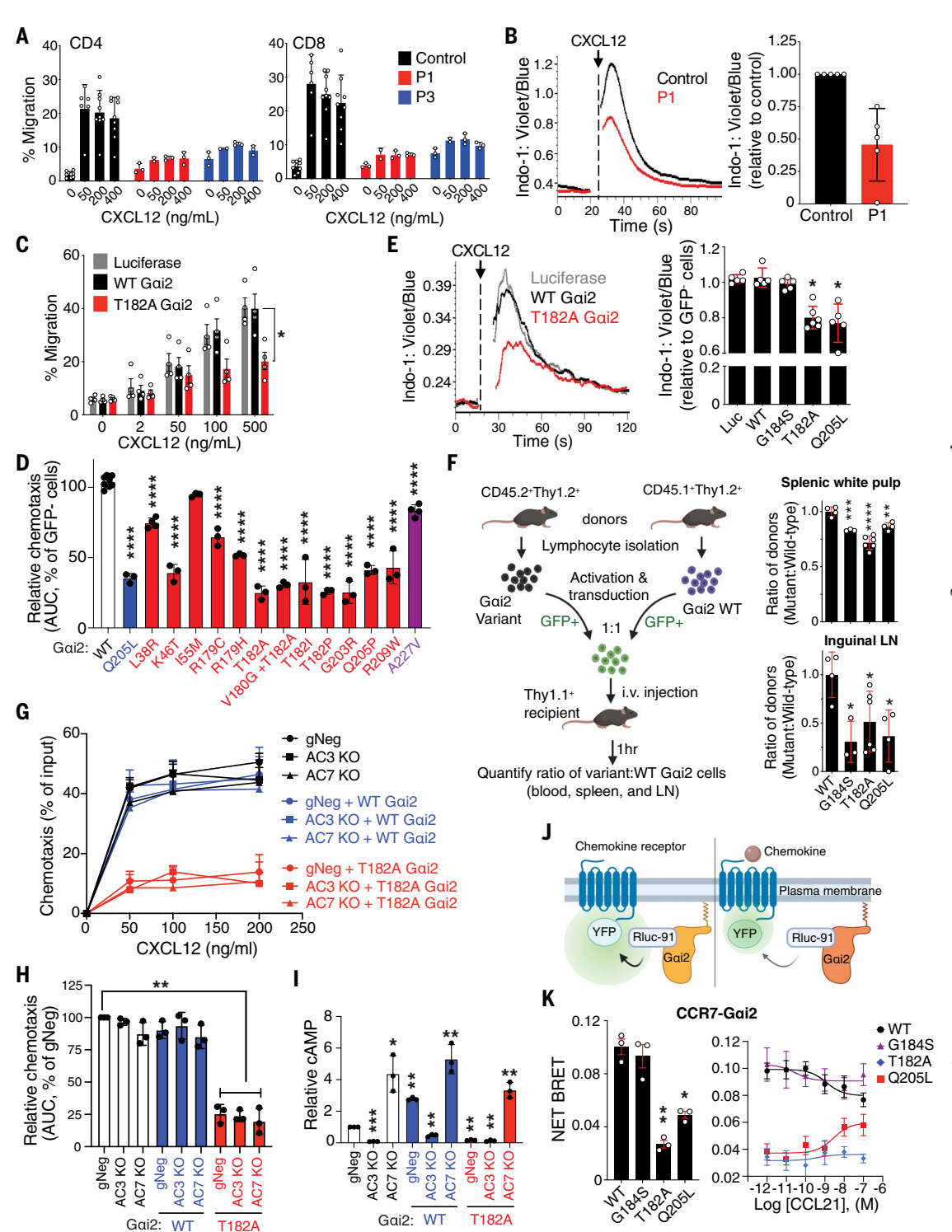
induced skin granulomas (c), psoriasiform rash (d), bronchiectasis (e), T cell infiltrates in lung (brown) (f) or brain (red) (g) in absence of infection. Intestinal malrotation (h). (**E**) Human phenotype ontology (HPO) summarized at top-level categories for each patient. Size of circle indicates number of phenotypes assessed for a patient within each category. No circle indicates fewer than two phenotypes assessed. Color scale indicates fraction of those phenotypes confirmed in a patient. Top-level categories were sorted from top to bottom according to the average fraction across patients. The proportion of immune phenotypes present was tested in patients having T182 mutations  $\{[n=6, \text{sample median } m=0.315, \text{SD}=0.145] \text{ compared with those without } [n=12, m=0.194, \text{SD}=0.131]; t(16)=1.788, P=0.046\}$  by a one-tailed two-sample t test. Patients 14 and 19 were removed from this analysis because patients 13 and 14 were related and patients 18 and 19 were related.

Using bioluminescence resonance energy transfer (BRET) to measure the interaction of  $G_{\alpha i2}$  proteins with GPCRs overexpressed in living cells, we found that the Thr<sup>182</sup> $\rightarrow$ Ala  $G_{\alpha i2}$  mutant found in patients and the Gln<sup>205</sup> $\rightarrow$ Leu activating mutant control protein showed minimal steady-state interaction with chemo-

kine receptors (Fig. 3, J and K, and fig. S12, A to C). Even with ligand engagement across a broad range of concentrations, the already low BRET intensity remained unchanged, in contrast to the high BRET signal that rapidly declined to similarly low levels in cells overexpressing WT G<sub>oi2</sub> (Fig. 3K and fig. S12A).

Increased dissociation from GPCRs also compromised chemokine-augmented suppression of transient cAMP production for several other patients' mutants (fig. S12, D and E). Hence, the more potent "active" mutant  $G_{\alpha i2}$  constitutively adopted a conformation that promoted decoupling from GPCRs, decreasing the pool

Fig. 3.  $G_{\alpha i2}$  mutants impair chemokine receptor signaling by decoupling from chemokine receptors. (A) Transwell migration to chemokines of T cells from patients or healthy donors. (B) CXCL12stimulated Ca<sup>2+</sup> fluxes from a patient or healthy donor T cells (left), quantified as area under the curve (AUC) and normalized to healthy donors (right). (C) Same as shown in (A) but using healthy donor T cells stably expressing  $G_{\alpha i2}$  variants or luciferase. (D) Same as shown in (C) but quantified by normalizing AUC of transduced (GFP+) cells to untransduced (GFP<sup>-</sup>) cells. (E) Same as shown in (B) using healthy donor T cells stably expressing  $G_{\alpha i2}$ variants or luciferase but quantified by normalizing AUC of transduced (GFP+) cells to untransduced (GFP-) cells. (F) (Left) Migration after adoptive transfer of mouse T cells stably expressing  $G_{\alpha i2}$ . (Right) Normalized ratio of variant to WT  $G_{\alpha i2}$ -transduced donor cells recovered from splenic white pulp or inguinal lymph node (LN). (G) Transwell migration of AC3 or AC7 KO human T cells also stably expressing  $G_{\alpha i2}$ variants or not. (H) AUC quantification of (G), normalized to gNeg-treated cells (gNeg is a nonspecific guide RNA). (I) FSK-induced cAMP in cells from (G). (J) Schematized BRET reaction between  $G_{\alpha i2}\text{-RLuc}91$  and GPCR-YFP. Ligand binding (right) results in a reduction of pre-ligand (left) BRET signal (green). (K) Net BRET signal between G<sub>qi2</sub>-RLuc91



and CCR7-YFP at basal conditions (left) or upon treatment with indicated chemokines (right). Gating strategies can be found in fig. S26A [for (B)], fig. S26B [for (E)], and fig. S26C [for (F)], and representative flow plots are presented in fig. S27A [for (F)]. Data show representative experiments [left, (B) and (E)]; means  $\pm$  SEM [(C) and (K)] or means  $\pm$  SD [(A), (B), and (E)] for three to six [(A) to (C), and (E)] or three (K) experiments; means  $\pm$  SD of two independent experiments [(F), total of three to five mice per group]; or means  $\pm$  SD of three experiments from one of two different donor-cell transductions [(D), and (G) to (I)]. Combined results from multiple experiments are shown, with each individual point representing a different blood draw obtained longitudinally from a given patient [(A) and (B)], an individual recipient mouse (F), or an independent experiment [(C) to (E), (H) and (I), and left panel of (K)]. Statistical analyses were performed using Kruskal-Wallis test with Dunn's multiple comparisons for (C) and (E); one-way ANOVA with Dunnett's multiple comparisons test for (D), (F), and (K); or one-sample t test with two-stage step-up method of Benjamini, Krieger, and Yekutieli for (H) and (I). \*t > 0.00; \*\*t > 0.001; \*\*\*t > 0.0001.

of GPCR-WT  $G_{\rm ci2}$  complexes able to recycle to active receptor complexes that can transduce GPCR signals for further biological responses.

Taken together, activating mutant  $G_{\alpha i2}$  proteins had the seemingly paradoxical effect of impairing responsiveness to chemokines and chemoattractants because the mutant  $G_{\alpha i2}$  proteins associate poorly to the receptors. This resulting impaired migration of immune cells can explain the patients' increased infection susceptibility.

# T cells from patients with mutant $\mathbf{G}_{oi2}$ proteins were hyperresponsive to TCR stimulation

Although impaired leukocyte migration could explain the patients' infection susceptibility, some patients also had life-threatening autoimmunity. Patients did not show decreased peripheral blood regulatory T cell or increased CD21<sup>lo</sup> CD38<sup>lo</sup> B cell numbers that could account for their autoimmunity (fig. S5, D and F). However, we noticed that overall lymphocyte proliferative responses to mitogens and antigens were not decreased but appeared normal or even higher than expected (fig. S6 and supplementary text 5).

We hypothesized that T cell hyperresponsiveness might explain the autoimmunity in patients. Therefore, we examined T cell behavior in vitro under various TCR-stimulating conditions. Similarly to our observations for gated T cells stimulated in peripheral blood mononuclear cell (PBMC) preparations (fig. S6), T cells purified from multiple patients (whether CD4+ or CD8+ T cells, or naïve or effector and memory T cells) exhibited enhanced induction of the activation markers CD69 and CD25 (IL-2 receptor  $\alpha$  subunit) and increased proliferation upon stimulation with anti-CD3 plus anti-CD28 antibodies compared with control samples (Fig. 4, A to F, and fig. S13, A to L). These differential responses were also seen when cells were stimulated suboptimally (anti-CD3 antibodies only) but were not apparent when cells were treated with more potent stimulation (beads consisting of immobilized anti-CD2, anti-CD3, and anti-CD28 antibodies). The presence of exogenously provided IL-2 throughout the experiments and normal IL-2 production by ex vivo CD4+ T cells (fig. S5E) suggested that the increased responses of the patient T cells did not result from increased IL-2 production.

To determine whether the increased T cell responsiveness was a direct effect of the mutant  $G_{\rm ci2}$  protein, we designed a guide RNA sequence (named gMP) that specifically knocks out the mutant but not the WT *GNAI2* allele of PI, using a CRISPR-Cas9 ribonucleoprotein (RNP) system (fig. S14, A to C). Treatment with gMP restored activation and proliferation of patient T cells to normal levels, indicating a positive role for the mutant protein in the increased T cell responsiveness (Fig. 4, G to I, and fig. S14, D and E). Transduction of CD4 $^+$ 

T cells from healthy normal donors with the Thr<sup>182</sup> $\rightarrow$ Ala or Gln<sup>205</sup> $\rightarrow$ Leu activating  $G_{ci2}$  mutants also increased TCR-induced responsiveness, which is similar to the results observed with patient T cells (Fig. 4, J and K, and fig. S13, M to Q), whereas partial knockout (KO) of  $G_{ci2}$  in T cells from healthy donors failed to do so (fig. S14, F to H). Thus, activating  $G_{ci2}$  protein—but not WT  $G_{ci2}$  protein—increased the stimulatory response to TCR engagement.

# Proteins involved in TCR signaling showed increased distal phosphorylation in cells with mutant $G_{\alpha i 2}$ proteins

T cell activation through the TCR initiates multiple signals that lead to rapid clonal expansion, including activation of the RAS proteins (HRAS, KRAS, and NRAS) facilitated by RAS guanyl-releasing proteins (RASGRPs) (26, 27). Activation of these small G proteins leads to activation of the extracellular signal-regulated kinase (ERK)/mitogen-activated protein kinase (MAPK) pathway, in parallel with the phosphatidylinositol 3-kinase (PI3K)-AKT-mechanistic target of rapamycin (mTOR) pathway (26, 27). Together, these signaling pathways promote a metabolic shift to aerobic glycolysis and an increase in protein synthesis for optimal cellular growth, proliferation, and differentiation. By contrast, overstimulation of these pathways can contribute to uncontrolled growth as seen in cancers, which have a high prevalence of somatic mutations in RAS, as well as certain leukoproliferative disorders associated with autoimmunity (28).  $G_{\alpha}$  proteins are canonically thought to function by modulating production of the second messenger cAMP (2). They mediate GPCR signaling mainly at the inner leaflet of the plasma membrane (PM) and may themselves be regulated during TCR activation (29, 30). Therefore, we examined how the mutant activating  $G_{\alpha i2}$  protein influences early events mediated by the TCR signaling complex at the PM. Previous work has shown that local cAMP at the PM of T cells stimulates the PKA-CSK pathway, which can counteract TCR signaling by deactivating the LCK nonreceptor tyrosine kinase (29-31).

We found that both freshly isolated and previously activated patient T cells showed normal. not increased, TCR proximal signaling (Fig. 5, A to D; fig. S15, A to D, and I to L; and fig. S16, A to D). However, the same cells showed enhanced distal phosphorylation of ribosomal S6 protein, a hallmark of growth and proliferation (Fig. 5, E to G; fig. S15, E, F, M, and N; and fig. S16. E. and H to J). S6 phosphorylation is mainly regulated by ERK/MAPK and PI3K-AKT signaling pathways (Fig. 5G, right) (32). Indeed, we observed enhanced and prolonged phosphorylation of ERK1/2 and p90RSK, as well as AKT and p70S6K, in patient T cells and in healthy donor CD4+ T cells transduced to express activating mutant  $G_{\alpha i2}$  proteins (Fig. 5,

G to L; fig. S15, G, H, O, and P; and fig. S16, F to J). Treating patient T cells with the PI3K/AKT/mTOR pathway inhibitor LY294002 and the MAPK kinase (MEK) inhibitor U0126 normalized S6 phosphorylation by preventing hyperactivation of AKT and p90RSK, respectively (fig. S17). Thus, active  $G_{\rm ci2}$  protein augments TCR-induced ERK/MAPK and PI3K/AKT/mTORC1 signaling pathways at a step unexpectedly downstream of proximal TCR signaling events.

# Mutant $G_{\alpha i2}$ modulated TCR-dependent signaling independently of cAMP

We determined that mutant  $G_{cii2}$  proteins from the patients inhibited AC-mediated cAMP production and that patient fibroblasts produced less cAMP (Fig. 1, H to J, and fig. S3). However, intracellular cAMP, when raised, generally plays suppressive roles in immune cells (30). Therefore, suppression of cAMP production by mutant  $G_{cii2}$  proteins might cause increased T cell responsiveness. We found that patient T cells produced cAMP at levels within the range of healthy donor T cells (Fig. 6A). This would be consistent with the major ACs expressed in primary human T cells being AC3, AC7, and AC9 (fig. S11, A and B), and which are not expected to show substantial regulation by  $G_{cii2}$  (6, 7).

To investigate the role of cAMP in T cell hyperresponsiveness further, we investigated whether manipulating cAMP levels could mimic or rescue the patient T cell phenotypes. KO of AC3 or AC7 in healthy donor T cells had elevated or decreased endogenous cAMP levels respectively, but neither affected TCR-induced S6-regulatory signaling, cellular activation, or proliferation (Fig. 6, B to F; fig. S11, C and D; and fig. S18). Furthermore, an exogenously added cAMP analog failed to normalize the increased responsiveness of patient T cells (fig. S19). Although these approaches did not specifically measure or manipulate local cAMP levels near the PM microdomain, the normal TCR proximal signaling in patient T cells suggests that G<sub>0i2</sub> may not affect local cAMP pools (Fig. 5, A to D; fig. S15, A to D, and I to L; and fig. S16, A to D).

Thus, our findings would be consistent with  $G_{\alpha i2}$  proteins regulating TCR signaling by means of cAMP-independent mechanisms.

# The interaction between $G_{\alpha i2}$ and RASA2 regulated TCR-dependent responses

To determine how hyperactive  $G_{\alpha i2}$  protein may regulate S6-regulatory signaling pathways through cAMP-independent mechanisms, we investigated  $G_{\alpha i2}$ -interacting proteins by performing affinity pulldown followed by quantitative mass spectrometry. For these experiments, we used  $G_{\alpha i2}$ -Thr $^{182}$  $\rightarrow$ Ala bound to GTP $_{\gamma}$ S as the bait protein, reasoning that relevant interactors might preferentially bind the active form of  $G_{\alpha i2}$ . We identified well-known and previously reported interactors of  $G_{\alpha i2}$  (e.g.,  $G_{\beta}$ 

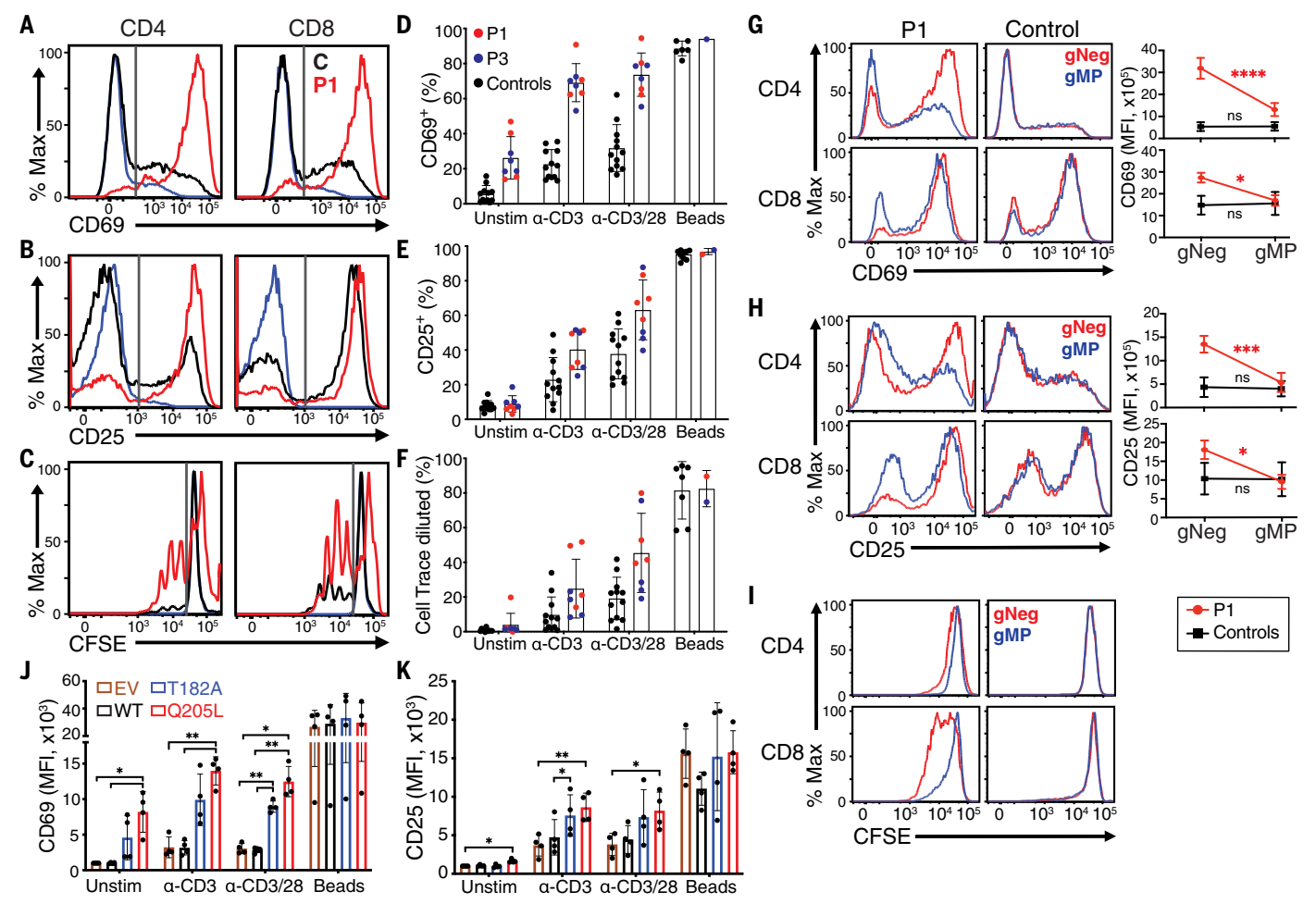


**Fig. 4.** Activating  $G_{\alpha i2}$  protein enhances T cell responses. (A to F) TCR-induced surface expression of CD69 [(A) and (D)], CD25 [(B) and (E)], and CFSE dilution [(C) and (F)] of naïve T cells purified from patient (P) or control (C) healthy donors. CFSE, carboxyfluorescein succinimidyl ester. [(A) to (C)] Representative histograms of gated CD4+ (left) and CD8+ (right) T cells from P1 (red) and C (black) stimulated with soluble anti-CD3 and anti-CD28 antibodies (1 μg/ml); blue indicates unstimulated C. [(D) to (F)] Quantification of CD69+ or CD25+ cells as % of gated CD4+ T cells from two patients and 12 controls. Each dot represents a different experiment with a different blood draw collected longitudinally over a span of 6 years. Unstim, unstimulated; α-CD3 or α-CD3/28, soluble anti-CD3 or anti-CD3 and anti-CD28 antibodies (1 μg/ml); Beads, bead-immobilized anti-CD2, anti-CD3, and anti-CD28 antibodies. (**G** to **I**) Same as shown in (A) to (F) using P1 or C T cells treated with indicated Cas9/ribonucleoprotein (RNP) and stimulated with anti-CD3 and anti-CD28

antibodies (0 to 1000 ng/ml; 100 ng/ml for representative histogram), except that mean fluorescence intensity (MFI) was measured. MFIs were plotted against doses of anti-CD3/28 (fig. S14D) to calculate AUC for each condition [right, (G) and (H)]. gNeg is a nonspecific guide RNA, and gMP targets the mutant GNAI2 allele of P1. (J and K) Same as (A), (B), (D), and (E), using CD4 $^+$ T cells stably expressing  $G_{cil^2}$  variants. EV, empty vector. Gating strategies can be found in fig. S26D [for (A) to (I)] and fig. S26E [for (J) and (K)]. Data show representative flow plots alongside combined results with means  $\pm$  SD for four [(A) to (F), (J), and (K)] or three [(G) to (I)] experiments. Two-way ANOVA was performed with Sidak's multiple comparisons, using cell type (C or P1) and gRNA target (gNeg or gMP) as factors for (G) and (H), or one-way ANOVA with Tukey's multiple comparisons test for (J) and (K). \*P < 0.05; \*\*P < 0.01; \*\*\*\*P < 0.001; \*\*\*\*P < 0.0001; \*\*\*\*P < 0.0001; ns, not significant (related data provided in figs. S13 and S14).

subunits, RGS, G protein–signaling modulator proteins, and RASA3), and previously unappreciated interacting proteins (including RASA2, PP2A-A $\alpha$ , and PP2A-C $\alpha$ ) (Fig. 6G and data S2). We did not detect any AC in our  $G_{\alpha i2}$ -interacting proteins, which would support the idea that the T cell–hyperresponsive phenotype may be regulated by cAMP-independent mechanisms.

RASA2, a member of the RasGAP (Ras GTPase-activating protein) family, was an intriguing candidate because its target, the RAS proteins, are major upstream regulators for the ERK/MAPK and PI3K pathways

(33, 34) that were augmented in the patients' T cells (Fig. 5). We confirmed the  $G_{ci2}$ -RASA2 interaction by coimmunoprecipitations from lysates of either cells overexpressing RASA2 and  $G_{ci2}$  proteins (Fig. 6H) or endogenously expressed proteins in patient T cells (Fig. 6I). Interactions of RASA2 with multiple different activating mutant  $G_{ci2}$  proteins were stronger than with WT  $G_{ci2}$ , suggesting that RASA2 might be an effector target of  $G_{ci2}$  (Fig. 6, H and I, and fig. S20A). Purified WT  $G_{ci2}$  protein directly bound RASA2 when loaded with GDP, but the interaction was markedly strength-

ened when loaded with GTP  $_{\!\gamma}\!S$  to "lock"  $G_{\!\alpha i2}$  in its active state (Fig. 6J).

We found that depletion of RASA2 in T cells from healthy donors enhanced TCR-induced S6-regulatory signaling pathways, cellular activation, and proliferation (Fig. 6, K and L, and fig. S20, B to D). These observations phenocopied the effects of activating  $G_{ci2}$  proteins and indicated that RASA2 normally negatively regulates these responses. Gene editing of P1 T cells revealed that KO of RASA2 augmented the T cell hyperactivation, which is consistent with the mutant  $G_{ci2}$  having delayed (but not

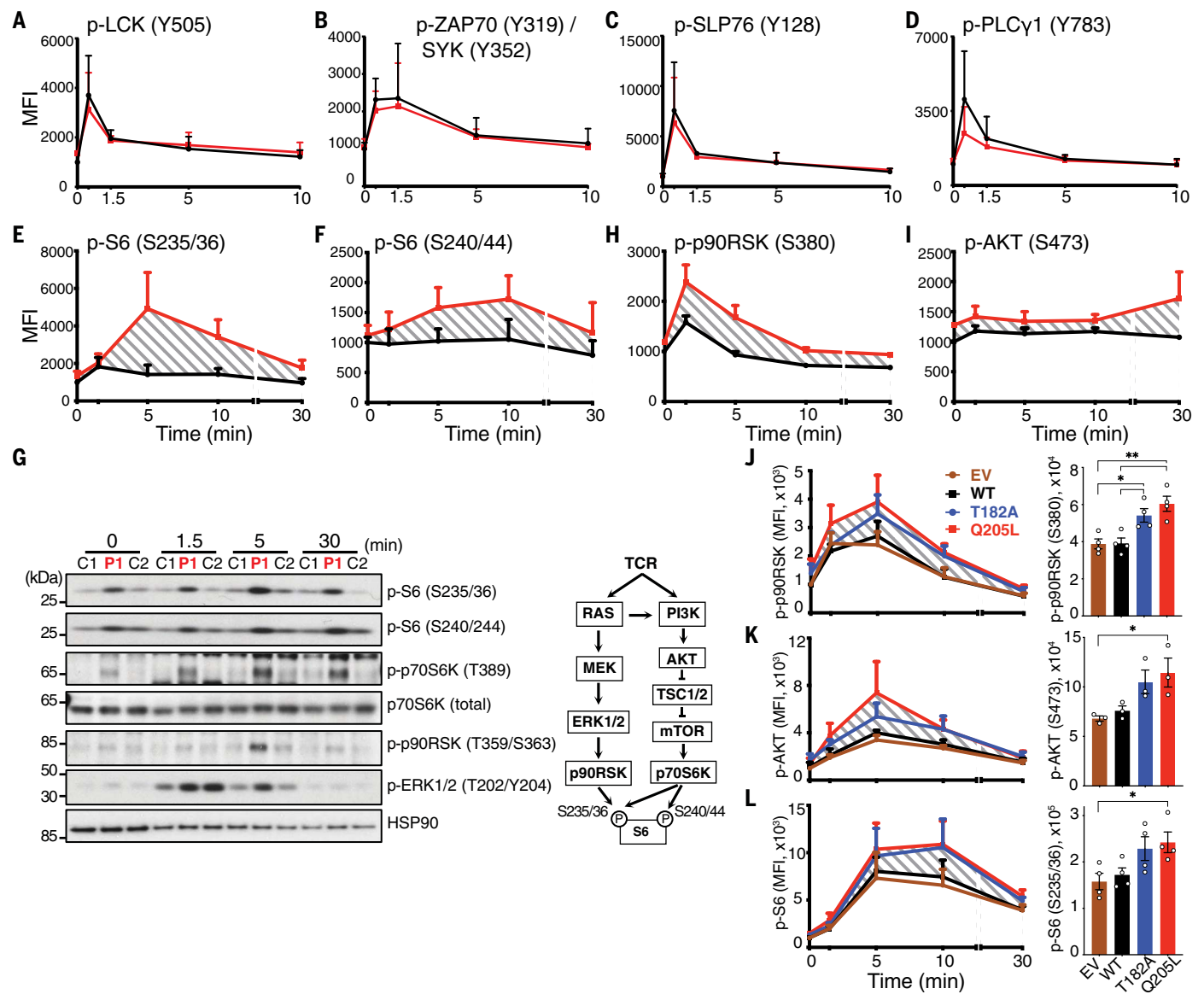


**Fig. 5.** Active  $G_{\alpha \mathbf{Z}}$  enhances TCR-induced S6-regulatory pathways. (A to I) Purified control (C) or patient (P1) T cells were activated with anti-CD3 antibodies for the indicated times, and samples were subjected to flow cytometry or immunoblot [(G), left]. Simplified diagram of TCR-induced signaling pathways is shown in (G), right panel. [(A) to (F), (H), and (I)] MFI was measured among the gated CD4<sup>+</sup> T cells. (**J** to **L**) Similar to what is shown in (A) to (I), using CD4<sup>+</sup> T cells from a healthy donor stably expressing  $G_{\alpha i2}$  variants and calculating AUC. EV, empty

vector. Gating strategies can be found in fig. S26F [for (A) to (F), (H), and (I)] and fig. S26G [for (J) to (L)]. Individual data points and representative flow plots are presented in fig. S27B [for (A) to (F), (H), and (I)] and fig. S27C [for (J) to (L)]. Data show a representative immunoblot (G), means  $\pm$  SEM [(J) to (L), right], or means  $\pm$  SD [(A) to (F), (H), and (I)], based upon three [(A) to (H), and (K)], two (I), or four [(J) and (L)] experiments. One-way ANOVA was performed with Dunnett's multiple comparisons test for (J), (K), and (L).  $^*P < 0.05; \, ^{**}P < 0.01.$ 

completely blocked) cycling upstream of RASA2 (Fig. 6M and fig. S21).

The levels of T cell hyperactivation in RASA2 KO T cells were comparable whether or not activated  $G_{\rm ci2}$  was also present (Fig. 6M and fig. S21). As the expression of the  $G_{\rm ci2}$  mutant did not further activate T cells in the absence of RASA2, it indicated that activated  $G_{\rm ci2}$  regulated these T cell responses completely or largely through RASA2.

These observations suggested a model in which activating  $G_{\alpha i2}$  proteins by binding RASA2 might relieve RASA2's negative regulation of

S6-regulatory signaling and T cell activation. Additionally, we identified and confirmed an interaction between active  $G_{ci}^2$  with PP2A Ser/Thr phosphatase complex members, PP2A-A $\alpha$  and PP2A-C $\alpha$  (Fig. 6G; fig. S20, E to I; and data S2). As PP2A negatively regulates both ERK/MAPK and p70S6K pathways, this interaction might reinforce the negative regulatory effects of RASA2 (35).

Thus, our data suggest that active  $G_{ci2}$  enhances T cell activation in a cAMP-independent manner by preventing negative regulation by RASA2 and/or the PP2A complex.

## Mutant $G_{\alpha i2}$ proteins sequestered RASA2 resulting in augmented RAS activity in T cells

Like  $G_{\rm ci2}$  and other G proteins, RAS functions according to its GDP- or GTP-bound states, and RASA2 suppresses RAS activation by accelerating RAS GTPase activity (33, 34). Patients' T cells consistently showed enhanced activation of RAS and downstream ERK1/2 upon TCR stimulation, suggesting that active  $G_{\rm ci2}$  limits RASA2 activity in T cells (Fig. 7A and fig. S22, A and B). To test whether RASA2's GAP activity toward RAS was inhibited by  $G_{\rm ci2}$ , we mixed purified recombinant RASA2

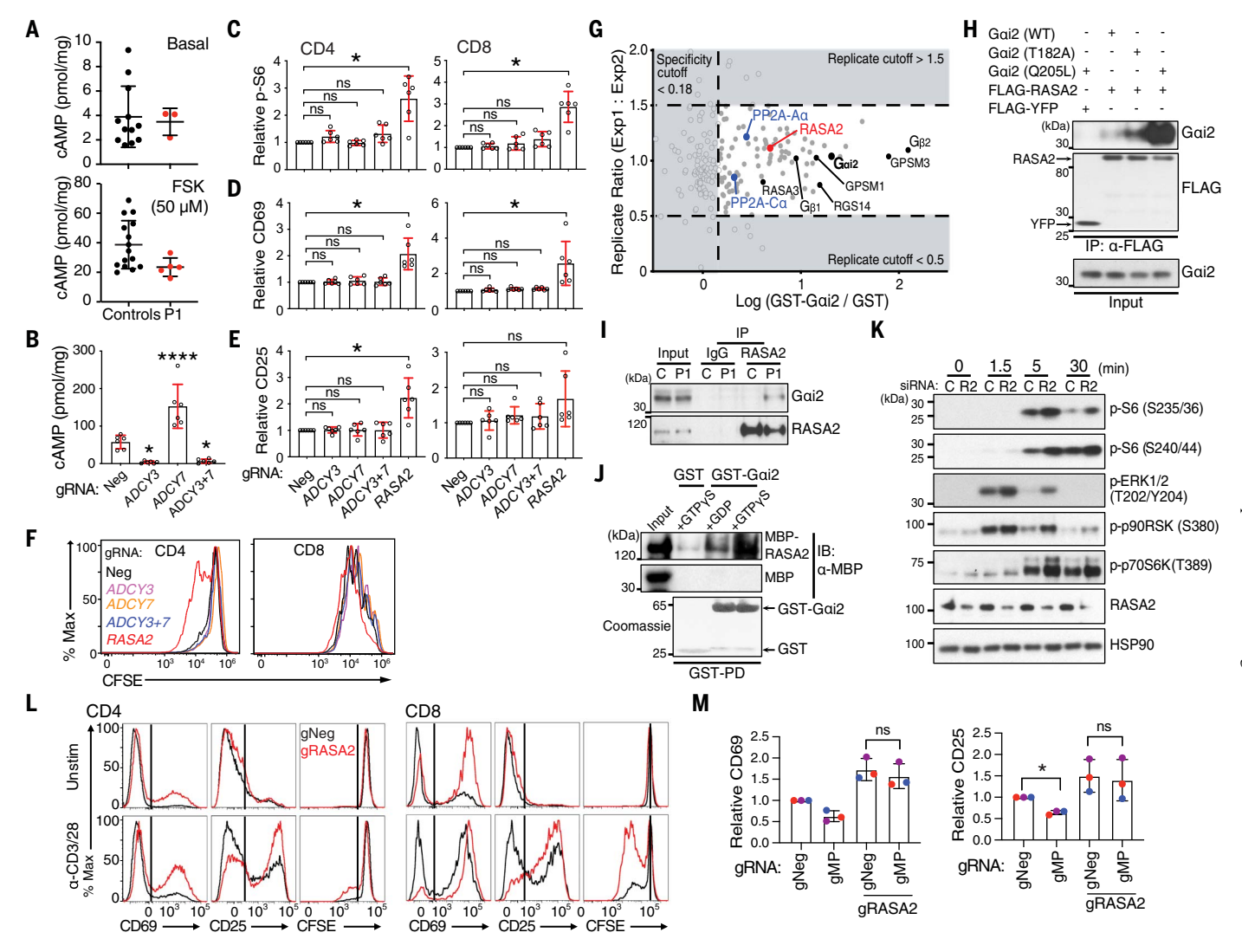


Fig. 6. RASA2, a G<sub>oi2</sub> effector target, constrains T cell responses. (A) cAMP accumulation in control or patient (P1) T cells at baseline (top) or upon stimulation with FSK (bottom). (B to F) T cells were transfected with indicated Cas9/RNP. (B) cAMP accumulation upon FSK treatment. [(C) to (F)] AUC quantification of TCR-induced S6 (S235/S236) phosphorylation (C), surface expression of CD69 (D) or CD25 (E), and CFSE dilution (F) on gated CD4+ or CD8+ T cells, relative to gNeg control, after flow-cytometric measurements of MFI. Cells were stimulated with anti-CD3 and anti-CD28 antibodies in (D) and (E) (0 to 1000 ng/ml) and in (F) (100 ng/ml). (**G**) Graphical representation of  $G_{\alpha i2}$ interacting proteins. Black indicates known interactors; red and blue indicate candidate interactors. (H) 293T cells were transfected as indicated. The FLAG peptide was immunoprecipitated (IP) and immunoblotted (labels on right side designate the specificity of antibodies used). (I) Immunoblot of RASA2 IP with T cell lysates from P1 or control (C). (J) Interaction between purified glutathione-S-transferase (GST)- $G_{\alpha i2}$  (loaded with either GDP or GTP<sub> $\gamma$ </sub>S) and maltose binding protein (MBP) or MBP-RASA2 fusion proteins through GST pulldown (PD). Coomassie staining was for GST-fusion proteins used in PD. IB, immunoblot. (K) Healthy donor T cells transfected with control (C) or RASA2targeting (R2) small interfering RNAs (siRNAs) were stimulated with anti-CD3 antibodies for varying times, and lysates were immunoblotted for indicated proteins. (L) TCR-induced surface expression of CD69 or CD25, and CFSE dilution of CD4<sup>+</sup> or CD8<sup>+</sup> T cells treated with gNeg (black) or gRASA2 (red) Cas9/RNP.

Cells were stimulated with anti-CD3 and anti-CD28 antibodies (100 ng/ml). (M) AUC quantification of CD69 (left) or CD25 (right) expression on gated CD4+ T cells, relative to gNeg control, after flow-cytometric measurements of MFI. Purified T cells from P1 were stimulated with increasing amounts of anti-CD3 and -CD28 antibodies (0 to 1000 ng/mL) after transfecting with the indicated Cas9/RNPs (gNeg, gMP targeting the mutant GNAI2 allele of P1, and gRASA2). Each colored dot indicates an experiment from a different blood draw. Gating strategies can be found in fig. S26F [for (C)], fig. S26D [for (D) to (F)], and fig. S26H [for (L) and (M)]. Representative flow plots are presented in fig. S27D [for (C)], fig. S27E [for (D)], fig. S27F [for (E)], and fig. S27P [for (M)]. Combined results from multiple experiments are shown, with each individual point representing an independent experiment [(A) to (E), and (M)]. Data show representative experiments [(F), and (H) to (L)] or means  $\pm$  SD [(A) to (E), and (M)], based on three [top panel in (A), (H) to (K), and (M)], five (L), five [(A), bottom], or six [(B) to (F)] experiments. (G) shows the analysis combined from two independent PD experiments. One-way ANOVA was performed with Dunnett's multiple comparisons test for (B); one-sample t test with two-stage step-up method of Benjamini, Krieger, and Yekutieli correction for multiple comparisons tes1t was performed with hypothetical value of 1 for (C) to (E); oneway ANOVA with Sidak's multiple comparisons test was performed to compare gNeg versus gMP, gNeg versus gRASA2, gNeg versus gRASA2+gMP, or gRASA2 versus gRASA2+gMP in (M). \*P < 0.05; \*\*\*\*P < 0.001; ns, not significant.

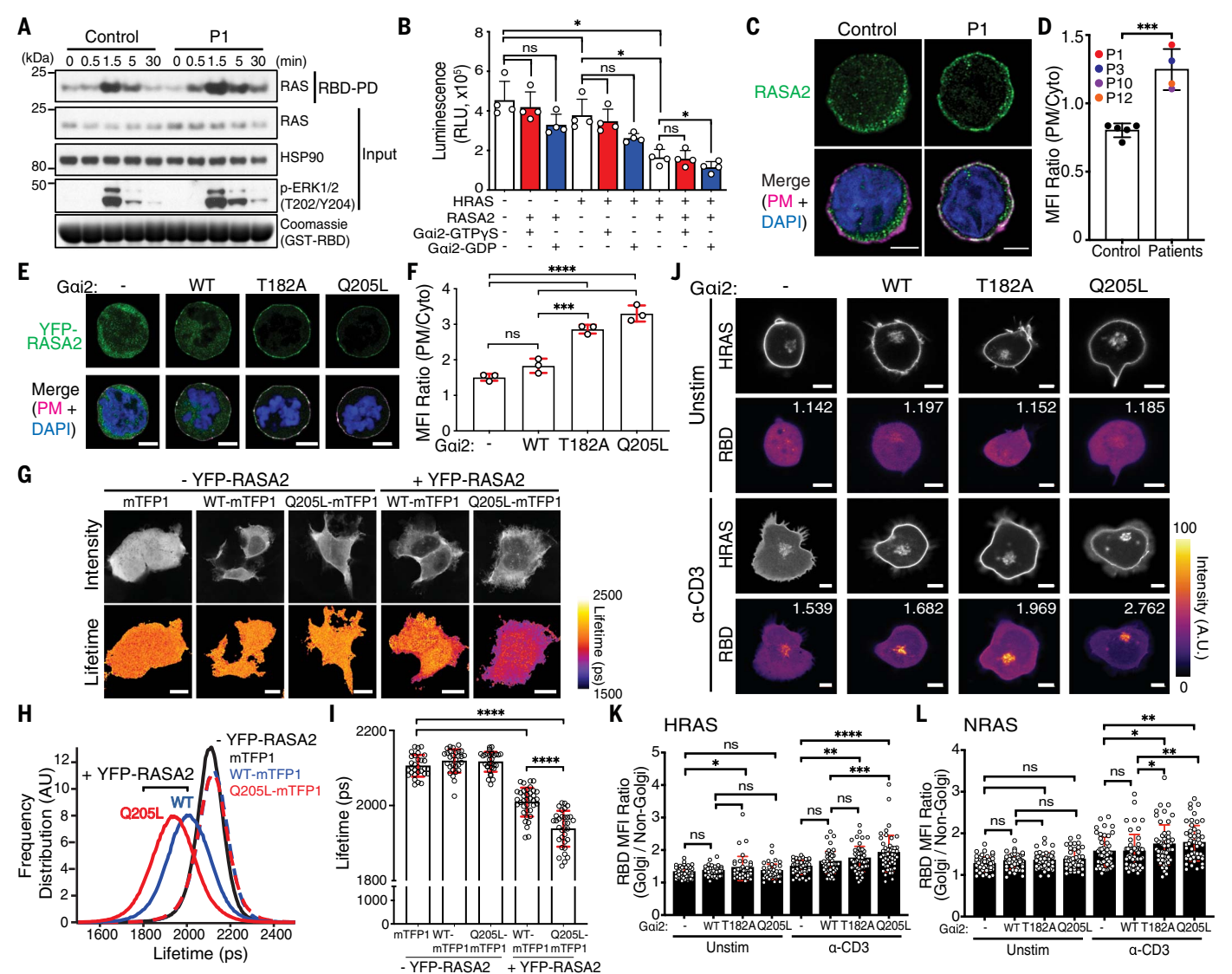


Fig. 7. Active  $G_{\alpha i2}$  promotes RAS activity by redirecting RASA2 to plasma membrane. (A) Control or P1 T cells were stimulated with anti-CD3 antibodies for varying times. Lysates were prepared for RBD pulldown (PD) to detect active RAS or for immunoblot for indicated proteins. Coomassie staining shows GST-RBD used in PD. (**B**) Purified HRAS, RASA2, and  $G_{\alpha i2}$  proteins (preloaded with GTP<sub>v</sub>S or GDP) were incubated as indicated with an excess of GTP. GTP consumption was determined by measuring remaining GTP level [represented by relative light units (RLU))]. (C) RASA2 distribution in CD4<sup>+</sup> T cells from P1 or healthy donor control. PM, plasma membrane. (D) MFI of RASA2 ratio at the PM relative to cytoplasm region (Cyto) in (C) and fig. S22D from four patients and five controls. (**E**) Distribution of YFP-RASA2 in  $G_{\alpha i2}$  KO Jurkats coexpressing indicated  $G_{\alpha i2}$ variants. (F) Quantification of (E) as shown in (D). (G to I) Fluorescence lifetime imaging (FLIM) of mTFP1 or G<sub>αi2</sub>-mTFP1 (WT, Q205L) with or without YFP-RASA2 expression in 293T cells. (G) Fluorescence intensity (top) and lifetime (bottom) of mTFP1. (H) mTFP1 fluorescence lifetime distribution. (I) Quantification of mTFP1 mean fluorescence lifetime. (J to L) Confocal microscopy colocalization analysis of unstimulated or TCR-induced active RAS distribution in  $G_{\alpha i2}$  KO Jurkats

transfected with enhanced green fluorescent protein (EGFP)-HRAS [(J) and (K)] or NRAS (L), mCherry-RBD, and Cerulean-GalT along with G<sub>ci2</sub> variants as indicated. (J) Number on RBD image represents MFI ratio of RBD at Golgi (defined by GalT stain) relative to non-Golgi region. [(K) and (L)] Quantification of RBD MFI ratio as in (J). Scale bar, 3 μm (C), 5 μm [(E) and (J)], or 10 μm (G). Data show representative or means ± SD for three [(A), (C) to (I), and (L)] or four [(B), (J), and (K)] experiments. Combined results from multiple experiments are shown in (B), (D), and (F), with each individual point representing an independent experiment [or a different patient in (D)]. Each individual circle in (I), (K), and (L) corresponds to the value from a different cell but with superimposed means ± SD from across multiple independent experiments. One-way ANOVA was performed with Tukey's multiple comparisons test for (B) and (F); an unpaired t test was performed for (D); two-way ANOVA was performed with mutant type and experiment as factors for (I); three-way ANOVA was performed with transfectant, stimulation, and experimental repeat as factors for (K) and (L) and Tukey's multiple comparisons test conditional on the stimulation status. \*P < 0.05: \*\*P < 0.01: \*\*\*P < 0.001: \*\*\*\*P < 0.0001; ns, not significant.

without or with active  $G_{\alpha i2}$  (loaded with  $GTP_{\gamma}S$ ), HRAS, and GTP, then measured RAS GTPase enzymatic activity through consumption of GTP. As GTP levels were unchanged by including active  $G_{\alpha i2}$ , these data suggest that  $G_{\alpha i2}$ 

did not directly inhibit RASA2's GAP activity toward RAS (Fig. 7B and fig. S22C).

We then considered the possibility that active  $G_{\rm ci2}$  could indirectly inhibit RASA2's GAP activity by altering its cellular location. Quantita-

tive confocal imaging in patients' cells or in cells overexpressing activating  $G_{\alpha i2}$  mutants revealed that active  $G_{\alpha i2}$  redistributed RASA2 toward the PM (Fig. 7, C to F, and fig. S22, D and E). By performing Förster resonance energy transfer

(FRET)-based fluorescence lifetime imaging, we examined whether this membrane recruitment of RASA2 is mediated by its interaction with  $G_{\alpha i2}$  (Fig. 7G). Fluorescence lifetime of a WT G<sub>ai2</sub>-mTFP1 FRET donor was quenched only in the presence of a YFP-RASA2 acceptor, indicating that the two proteins are closely apposed (within 10 nm) (Fig. 7, G to I) (mTFP1, monomeric teal fluorescent protein from Clavularia coral). Quenching was mainly observed at the cell periphery near the PM, with FRET efficiency reciprocally also increased there (fig. S22F). The mTFP1 lifetime was dramatically shorter when the activating  $G_{\alpha i2}$  mutant  $Gln^{205} \rightarrow Leu$ was coexpressed with RASA2 (red versus blue color in Fig. 7H), with FRET efficiency also increased under the same conditions (fig. S22F), supporting an increased association between these two proteins.

In T cells, exogenously expressed HRAS or NRAS localizes to both the PM and Golgi, but RAS activation predominates at the Golgi during TCR activation (26, 36). Therefore, we assessed whether RAS activation at the Golgi correlates with  $G_{\alpha i2}$ -mediated RASA2 redistribution to the PM after TCR stimulation. Using Jurkat cells coexpressing fluorescently tagged RAS, active-RAS sensor (RBD), and a Golgi marker (GalT), along with  $G_{0i2}$  proteins, we performed confocal microscopy colocalization analysis. We observed greatly enhanced RAS activation at the Golgi when cells expressed an activating mutant  $G_{\alpha i2}$  versus normal  $G_{\alpha i2}$ (intensity ratio 2 to 2.8 versus 1.7) (Fig. 7, J to L, and fig. S22, G to I).

PI3K-AKT activation is PM-restricted, so the enhanced PI3K-AKT signaling in the patient T cells implied that PM RAS activity was also increased (Fig. 5, I and K; figs. S15, H and P; S16, G to I; and S17) (37). Because both RAS and  $G_{ci2}$  at the PM undergo dynamic spatiotemporal regulation,  $G_{ci2}$ -mediated RASA2 sequestration might also enhance local RAS activity within the PM microdomains (29, 34). Overall, our findings suggest that active  $G_{ci2}$  enhances TCR-induced RAS activity by physically directing RASA2 away from RAS within cells.

#### Discussion

Previously, activating mutations in other  $G_{\alpha}$  subunits have been reported in various types of human cancers and diseases, and investigations have focused on their augmented downstream signaling pathways (38, 39). By studying humans with activating GNAI2 mutations, we found enhanced suppression of effector cAMP generation and established a pathogenic role of chronic decoupling of active  $G_{ci2}$  from GPCRs. Chronic decoupling can result from multiple factors, such as faster GTP binding, slower intrinsic hydrolysis, and RGS insensitivity. When compounded, these factors could disproportionately prolong the time

G proteins take to cycle from their active free form back to their inactive GPCR-bound form that is capable of responding again to GPCR agonists. Rapid G protein cycles may be required to respond to quickly changing environmental cues, such as for optimal spatiotemporal sensing of chemokine gradients through  $G_{ci}$  during cell migration. A similar requirement apparently underlies rapid photoreceptor deactivation to detect sudden changes in moving objects through  $G_{cit}$  during spatiotemporal visual signaling (40). Nevertheless, we do not exclude a possible additional contribution of active  $G_{cit}$  through sequestering or otherwise interfering with free  $G_{\beta\gamma}$  signaling (21, 41–44).

Although we have established that the impaired migratory behavior of immune cells leads to the patients' infection susceptibility and immune dysregulation, the additional clinical features of the patients suggest that the migratory behavior of nonimmune cells is similarly impaired during development The patients' prominent midline anatomic defects may reflect abnormal neural crest cell migration, which proceeds along the anteriorposterior axis during embryogenesis to help form many tissues (45). Such migration requires CXCL12 signaling through the CXCR4 chemokine receptor, whose deficiency causes cerebellar and other anatomical abnormalities and is embryonically lethal in mice (46). Furthermore, partial knockdown of Gnai2 in developing mouse embryos perturbed neuronal migration during corticogenesis, which is consistent with Gai2 regulating differentiated nonimmune cell migration during development and paralleling defective leukocyte migration in Gnai2 KO mice (15, 47). Unfortunately, we could not track migration of non-immune cells during development because attempts to generate a patient-mimicking knock-in (KI) mouse model were unsuccessful.

Besides establishing an important physiologic requirement in vivo for the normal cycling of  $G_{\alpha i2}$  during cell migration, our patients with constitutively activating mutant G<sub>0i2</sub> reveal a Gqi2-mediated but cAMP-independent RASregulatory pathway that controls the amplification of T cell responses through RASA2. We now place  $G_{\alpha i2}$  immediately upstream of RASA2 at the nexus of GPCR and TCR signaling pathways. In healthy individuals, this pathway could operate physiologically when G<sub>012</sub> is transiently activated by chemokine receptors, to coordinate T cell migration with and optimize TCR-induced activation and proliferation. Such a model may be consistent with the previously reported costimulatory contribution of chemokine receptor signaling during T cell activation (48). In patients with activating GNAI2 mutations, we propose that the resulting stronger TCR input breaks peripheral tolerance, predisposing them to the autoimmunity and age-associated lymphocytosis seen in some individuals. Exploiting this Gai2-RASA2-RAS signaling axis could facilitate development of T cell-based antitumor therapies. For example, improving expansion and activity of T cells expressing chimeric antigen receptor (CAR) could be achieved by fusing CAR to mutant G<sub>ci2</sub> domains that preferentially scavenge RASA2 (49). Indeed, our observations support recent studies with CRISPR screens in primary T cells and mouse models of cancer immunotherapy that provide evidence of RASA2 as a negative regulator (50, 51). As KO of RASA2 in transgenic CD8+ T cells or CAR T cells increases antigen-specific tumor cell killing in vitro (50, 51), those results suggest that a similar approach targeting G<sub>oi2</sub> upstream of RASA2 might also be promising.

There are several limitations to our study. First, we focused on the impact of the patients' GNAI2 mutations on their  $G_{\alpha i2}$  proteins and not on  $G_{\beta\gamma}$  proteins. Their activating  $G_{\alpha i2}$  mutants are expected to not only decouple from GPCR but also to increase dissociated  $G_{\beta\gamma}$ . Free  $G_{\beta\gamma}$  signaling regulates chemokine-mediated cell migration by modulating phosphoinositide-3-kinase γ (PI3Kγ) and possibly AC activities (52). However, one of our patients had an Arg<sup>209</sup>→Trp activating mutation in the "Gly-Arg-Glu" triad, which is required for  $G_{\beta\gamma}$  dissociation from  $G_{\alpha}$  for other G proteins (21). This variant is predicted to have the opposite effect of decreasing free  $G_{\beta\gamma}$ , yet it was still associated with impaired leukocyte migration. Therefore, although the activating  $G_{oi2}$ mutants could also exert secondary effects through increased free  $G_{\beta\gamma}$ , this explanation does not account for our observations. Studies addressing the impact of the activating  $G_{\alpha i2}$ mutants on  $G_{\beta\gamma}$  biology, including downstream spatiotemporal effects on cell polarity, adhesion, and migration, will be needed to clarify

A second limitation of our study is that although we have shown that activated  $G_{\alpha i2}$  acts primarily through RASA2 to drive RAS-mediated T cell hyperresponsiveness, the effect conferred by RASA2 KO was greater than that conferred by activating G<sub>0i2</sub> alone. Several factors may account for this difference. Constitutively activating Gai2 mutants are expected to have prolonged cycling but still pass through an inactive form, which binds less well to RASA2. In our experiments, we tested Thr<sup>182</sup>  $\rightarrow$  Ala, but other variants having different cycling times may show different relative effect sizes. Furthermore, the relative amounts of active  $G_{oi2}$ versus RASA2 in the cells and the stoichiometry required for efficient sequestration away from the Golgi are unknown. Alternatively, Gqi2-independent factors could also regulate RASA2. Additional studies are needed to address these possibilities.

Lastly, on the basis of their activated RAS-MAPK signaling, patients with germline-activating

GNAI2 mutations can now be included within the RASopathy spectrum (53, 54). Indeed, our patients show clinical overlap, including autoimmunity, with patients having typical RASopathies such as Noonan syndrome (53, 55). The widespread tissue expression of  $G_{\alpha i2}$  and RASA2, along with the diverse biological functions mediated by RAS proteins in cancer pathogenesis, raises the interesting possibility that the G<sub>012</sub>-RASA2-RAS signaling axis might broadly regulate growth, proliferation, and differentiation in the body. Consistent with this possibility, inhibitory roles of RASA2 in cellular growth and proliferation have been reported in fibroblast and melanoma cells (56). Additionally, somatic activating GNAI2 mutations have been identified in cancers including melanoma, adrenal cortical tumors, and ovarian sex cord-stromal tumors (39, 57), paralleling loss-of-function RASA2 mutations in melanomas and dysregulated RAS activity in various human cancers (33, 34, 56, 58). Thus, our discoveries also provide fresh insight into the molecular etiology and potential therapeutic targets to disrupt  $G_{\alpha i2}$  for tumors with oncogenic GNAI2 or RAS pathway mutations.

#### **Materials and methods**

#### Study participants and human sample collection

The patients originated from diverse ethnicities/ geographic regions (Latino/Admixed American, Non-Finnish European, European-Finnish, West Sub-Saharan African, Middle Eastern Arab). Age and sex of patients are contained in supplementary text 4. All enrolled subjects (patients, family members, healthy donors) provided written informed consent to participate in local Ethics or IRB-approved research protocols from various institutions (see supplementary materials for details). Patient or parent/legal guardian provided additional written authorization for publication of potentially identifiable facial photographs. Whole blood samples, fingernail clippings, skin punch biopsies, blister fluid, mouth washings, and skin swabs were obtained for experimental analyses in accordance with research protocols.

#### Mice

Animal housing, care, and experimental procedures of mice (*Mus musculus*) were performed under animal study protocols approved by the NIAID Animal Care Use Committee or the Garvan Institute of Medical Research/St. Vincent's Hospital Animal Ethics Committee. Mouse euthanasia was performed by carbon dioxide inhalation followed by cervical dislocation. Wildtype (WT) B6 (C57BL/6J, strain# 000664), CD45.1 congenic B6 (B6. SJL-Ptprca Pepcb/BoyJ, strain# 002014), and Thyl.1 congenic B6 (B6.PL-Thyla/CyJ, strain# 000406) were purchased from the Jackson Laboratory (Bar Harbor). Adoptive transfer experiments used female mice at 6 to 8 weeks

of age. Generation of *Gnai2* KI embryos was as described in the supplementary materials and methods.

# Whole-exome sequencing, whole-genome sequencing, and analyses

We conducted whole-exome sequencing (WES) on the index patient (P1) and her healthy parents and sister. Patients 2 to 18 and 20 with mutations in the GNAI2 gene were identified from WES or whole-genome sequencing (WGS) data (14), either through GeneMatcher (phenotype-agnostic) or through other inquiries that were broadly immune phenotype driven (59). Exome or genome libraries from gDNA were generated, and variant calling and analysis performed using various platforms (see supplementary materials for details). The familial GNAI2 mutation in P19 was identified by Sanger sequencing. In the patients, no other candidates besides GNAI2 were shared under de novo, autosomal recessive (AR), or variable-penetrance autosomal dominant (AD) models of inheritance (table S1). All genomic variants in this manuscript are described according to Human Genome Variation Society recommendations (60), using GenBank Reference Sequences NC 000003.11(gDNA), NM 002070.2 (mRNA), and NP 002061.1 (protein) based upon genome assembly Build GRCh37 unless otherwise indicated.

# Characterization of $G_{\alpha i2}$ GTPase and RASA2 GAP activities

For GTP binding and hydrolysis assays, recombinant G<sub>012</sub> protein was mixed with BODIPY-FL-GTP or BODIPY-FL-GTP<sub>γ</sub>S (Thermo Fisher), and the kinetics of in vitro  $G_{\alpha i2}$  protein activation measured (61). To examine RGS sensitivity,  $G_{\alpha i2}$  was incubated with RGS16 before adding BODIPY-FL-GTP. Nucleotide-binding data were fit with one phase exponential equation  $F = a - b e^{-kt}$ , where F is a specific increase of fluorescence, to obtain k GTP binding and hydrolysis curves were fit with the equation  $F = (C_0 k_1 / (k_2 - k_1)) (e^{-k_1 t} - e^{-k_2 t})$  for the intermediate product in two sequential reactions (62). For RGS binding assays, recombinant His6-Gai2 and GST-RGS16 were incubated together at 4°C in the presence of a slurry of glutathione sepharose beads and either GDP or GDP plus aluminum magnesium fluoride (AMF) to mimic the transition state for GTP hydrolysis (18). Bound proteins were eluted from beads, resolved by SDS-PAGE, and immunoblotted, GAP activity of RASA2 toward RAS protein was measured according to manufacturer's instructions (Promega), with modifications. Unless stated otherwise, 1 µM His-tagged hRas (Cytoskeleton, Inc.), 0.25 µM maltose binding protein (MBP) or MBP-RASA2, and 2.5 µM GST or GST-Gai2 proteins, pre-loaded with either GDP or GTP, S, were incubated with 5  $\mu M$  GTP and 1 mM DTT in the provided GTPase/GAP Buffer. Levels of GTP remaining were measured.

#### Cells, media, and cell culture

Human embryonic kidney (HEK) 293T cells (HEK293T), HEK293 cell line stably lacking AC3 and AC6 (HEK-AC $\Delta$ 3/6) (63), Platinum-E cells, NIH/3T3, Jurkat T cells, and HL60 cells were cultured in DMEM or RPMI 1640 medium with supplements. PBMCs were isolated from whole blood by Ficoll-Paque PLUS density gradient centrifugation (Cytiva). Pan-T cells or CD4+ T cells were isolated from PBMCs by negative selection (Miltenyi Biotec), or by fluorescence-activated cell sorting (FACS) using a BD FACSAria III cell sorter. For functional studies, purified T cells were used either immediately or activated using the T Cell Activation/Expansion Kit (Miltenyi Biotec). The latter were expanded in the presence of 100 U/mL recombinant human IL-2 for 2 to 3 weeks before use. Neutrophils were isolated by density gradient separation and used immediately for experiments. Fibroblasts were isolated from skin punch biopsies and cultured as described (64). Murine leukocytes isolated from spleens, inguinal and axial lymph nodes were activated with plate bound antimouse CD3 (5 µg/ml) and soluble anti-mouse CD28 (1 ug/ml) and cultured in RPMI medium containing 100 U/ml recombinant human IL-2.

#### cAMP measurements

293T cells (previously transfected with individual  $G_{\alpha i2}$  plasmid using polyethylenimine) or human dermal fibroblasts were stimulated at 37°C for 20 min with 5 µM FSK in the presence of 0.5 mM of the nonspecific inhibitor of phosphodiesterase 3-isobutyl-1-methylxanthine (IBMX). In some experiments, T cells (10 to 20 days after initial activation) were stimulated with 50 µM FSK and 0.5 mM IBMX at 37°C for 20 to 60 min. Cells were lysed and accumulated intracellular cAMP levels measured using the colorimetric cAMP ELISA Kit per manufacturer's instructions (Cell Biolabs). cAMP was alternatively measured using a YFP-Epac-rLuc cAMP biosensor (pcDNA3L-His-CAMYEL) in 293T cells previously transfected also with plasmids expressing  $G_{\alpha i2}$  and CXCR4 (65). Cells were stimulated in BRET Buffer (0.5 mM MgCl<sub>2</sub> and 0.1% BSA fraction V in PBS) with FSK  $(0, 10^{-8} \text{ to } 10^{-4} \text{ M})$  in the presence of 5  $\mu$ M Coelenterazine h for 10 min at room temperature. Luminescence and fluorescence readings were collected by sequential integration of the signals detected in the  $480 \pm 20$  nm and 530 ± 20 nm windows for luciferase (Rluc) and YFP light emissions, respectively. Relative cAMP levels were indicated as 1/BRET (Rluc/ YFP). In some experiments, 293T cells were transfected 24 hours previously with Gai2 plasmid and cAMP GloSensor reporter plasmid. Luminescence was measured at baseline and for 60 min after cells were treated with 2.5  $\mu M$  FSK.

#### Clinical phenotyping and analysis

Using criteria standardized across the patient cohort, clinical histories were coded into Human Phenotype Ontology (HPO) terms (66) and dysmorphology terms (defined at https://elementsofmorphology.nih.gov/index.cgi). For an individual patient, a value of "yes," "no," "ND" (not determined), or "NA" (not applicable, because of age or sex) was assigned to each HPO term (see data S1). Values were used to compute frequencies across the cohort for each HPO term. Selected midline (fig. S4A) or immune (fig. S4B) phenotypes were displayed as heatmaps, and phenotypes were also summarized at different level HPO categories.

#### T cell migration assays

Migration of T cells from patients and healthy donors 12 to 24 days post-activation, or of  $G_{\alpha i2}$ WT- or variant-transduced healthy donor T cells, was assessed in vitro using a standard Transwell system with 5 µm membrane pore inserts. Recombinant human CXCL12 or CCL21 was added to the lower compartment with an equivalent number of CountBright Absolute Counting Beads (Thermo Fisher) to each well. After incubating at 37°C for 2 hours, the contents of the lower chamber were collected and stained with antibodies for flow-cytometric analysis. The number of recovered cells was normalized to the number of CountBright Absolute Counting Beads collected, Migrated cells were expressed as % of the total number of cells collected from a well without a Transwell insert. Chemotaxis was calculated by subtracting random migration (determined by the wells without added chemokines). For in vivo assessment of T cell migration, wildtype (WT) C57BL/6 mice were purchased from the Jackson Laboratory (Bar Harbor). Mouse CD45.1+Thy1.2+ and CD45.2+Thy1.2+ lymphocytes were activated and transduced with retroviral particles containing MSCV-GFP-T2A-GNAI2 (WT) or MSCV-GFP-T2A-GNAI2 (WT or variants), respectively. Transduced cells (mixed 1:1) were intravenously injected into CD45.2 Thy1.1 \* recipient mice, followed by anti-CD5 PE/Cy7 1 hour later to label leukocytes in the splenic red pulp and the blood (67), and euthanized 3 min later. T cells recovered from tissues and blood were identified as donor (Thy1.2+GFP+), WT  $G_{\alpha i2}$  transduced cells were distinguished as CD45.1<sup>+</sup>Thy1.2<sup>+</sup>GFP<sup>+</sup>, and variant  $G_{\alpha i2}$  transduced cells were CD45.2 Thy1.2 GFP+. The normalized ratios of variant to WT  $G_{\alpha i2}$  transduced cells were calculated by normalizing for differences in transduction efficiencies of each donor cell prep, migration differences between the nontransduced CD45.1+Thy1.2+ and CD45.2+Thy1.2+ populations, and the WT  $G_{ci2}$  (CD45.1+Thy1.2+) vs. WT  $G_{oi2}$  (CD45.2<sup>+</sup>Thy1.2<sup>+</sup>) control group mice (average of these mice was set to a ratio of 1).

#### Neutrophil migration assays

Where neutrophils could be isolated freshly from patients and tested within 24 hours, their migration to buffer or N-formylmethionine leucyl-phenylalanine (fMLP) was measured ex vivo at 37°C using EZ-TAXIScan instrumentation (Effector Cell Institute, Tokyo, Japan) as described (68). Alternatively,  $G_{\alpha i2}$  WT- or varianttransduced HL60 cells were differentiated with 1.3% DMSO for 5 days, and their migration to fMLP, CXCL12, or leukotriene B4 (LTB4) was similarly assessed. Digital images of migrating cells were captured every 15 to 30 s for 30 min to 1 hour for quantitative analysis. In some experiments, migration to fMLP of DMSOdifferentiated,  $G_{\alpha i2}$ -transduced HL60 cells was also evaluated using the Transwell system. In vivo migration into cutaneous blister fluid of P1 and healthy donors was evaluated 16 hours after applying a suction blister device to skin as described (69), or in the oral cavity of subjects using a timed (10-s) oral rinsing procedure with 10 ml of sterile saline (0.9% Sodium Chloride) (70). The cell pellets from either blister exudate or oral cavity rinses were stained with a combination of anti-human antibodies for quantitative flow-cytometric analysis.

### Measurement of chemokine receptor– $G_{ci2}$ interactions

293T cells, previously transfected with CXCR4-YFP or CCR7-YFP acceptor plasmids and  $G_{\alpha i2}$ -Rluc donor plasmid, were stimulated in BRET buffer for 5 min at 37°C with increasing amounts of CXCL12 or CCL21 before adding 5  $\mu$ M Coelenterazine h. Luminescence and fluorescence readings were collected, and net BRET values were calculated by subtracting the background BRET signal from cells expressing only BRET donor ( $G_{ci2}$ -Rluc).

#### TCR stimulation

Purified human T cells were stimulated in complete RPMI medium and 100 U/ml recombinant human IL-2, using 1 µg/ml soluble antihuman CD3 (α-CD3), 1 µg/ml soluble anti-CD3 and anti-CD28 antibodies (α-CD3/28), or beads with immobilized anti-CD2, anti-CD3, and anti-CD28 antibodies (Beads; at 1:1 bead to cell ratio; Miltenyi Biotec). In some cases, cells were previously stained with carboxyfluorescein succinimidyl ester (CFSE) or CellTrace Violet. Flow cytometry was used to analyze CD69 expression at 20 hours, or CD25 expression and CFSE dilution at 96 hours after stimulation. For transduced CD4+ T cells or Cas9/RNP transfected T cells, cells were stimulated with  $\alpha$ -CD3/28 (0 to 1000 ng/ml), and CD69 and CD25 were examined at 18 to 20 hours later. For biochemical experiments, T cells were rested in serum-free RPMI at 37°C for 1 hour, incubated with 5  $\mu$ g/ml  $\alpha$ -CD3 in serum-free RPMI containing 0.5% bovine serum albumin (BSA) on ice for 10 min, followed by addition of 20  $\mu$ g/ml of goat anti-mouse IgG antibodies at 37°C for 0 to 30 min. To stop stimulation, cells were washed with ice-cold PBS, and either lysed for immunoblot or active RAS pulldown, or fixed for flow-cytometric intracellular staining. In some experiments, inhibitors (3  $\mu$ M LY294002, 10  $\mu$ M U0126, or DMSO) were added 1 hour prior to, or the cAMP analog 8-CPT-cAMP 15 min prior to, T cell stimulation.

#### Gene KO by CRISPR-Cas9 RNP system

Cas9/RNP complexes were prepared according to manufacturer's instructions (IDT) (71) and transfected using a 4D nucleofector system into primary human T cells (P2 solution, program EH-100) or Jurkat T cells (SE solution, program CL-120). The total amount of transfected gRNA per nucleofection was kept constant by adding gNeg RNA as needed. CRISPR-Cas9-mediated KO efficiency was evaluated by immunoblotting or estimated via TIDE assay (72). For evaluation of the patient's mutant allelespecific KO, cDNA was isolated and subjected to Sanger dideoxy sequencing. Experiments were performed 6 to 7 days after transfection.

#### GST pulldown assays and mass spectrometry analysis

Glutathione S-transferase (GST)-fused G<sub>ci2</sub> proteins bound to glutathione (GSH)-agarose resin were loaded with 500 mM GDP or GTP<sub>v</sub>S and washed before use. For pulldown assays, MBP fusion proteins were prepared in pulldown buffer (lysis buffer with 500 uM GDP or GTP<sub>v</sub>S and 20 mM MgCl<sub>2</sub>), incubated with prepared GST fusion protein-bound resin, and interacting proteins were eluted for immunoblotting. Active Ras pulldown assays were performed according to manufacturer's instructions (Cytoskeleton, Inc.). For mass spectrometry analysis, clarified Jurkat T cell lysates prepared in pulldown buffer were incubated with GSTor GST-G<sub>012</sub>(Thr<sup>182</sup> → Ala)-bound resin in the presence of GTP<sub>v</sub>S. Bound protein complexes were eluted and resuspended in acid extractable detergent. Samples were trypsin-digested and labeled with different isotopes using "reductive dimethylation" essentially as described for protocol C (73). Samples were mixed and a single long liquid chromatography with tandem mass spectrometry (LC-MS-MS) experiment was performed using the EASY-nLC 1000 Liquid Chromatograph interfaced with a Orbitrap Fusion Lumos Tribrid Mass Spectrometer (Thermo Fisher). Data were analyzed using MaxQuant (74) specifying 0 missed sites to decrease digestion difference based variation at an FDR of 1%. Mass spectrometry proteomics dataset was submitted to the ProteomeXchange Consortium via the PRIDE (75) partner repository (identifier PXD048980 and 10.6019/PXD048980).

#### Microscopy

Human CD4<sup>+</sup> T cells or G<sub>αi2</sub> KO Jurkat T cells transfected with plasmids expressing YFP-RASA2 and  $G_{\alpha i2}$  were stained with CellBrite® Fix 555 PM dye (Biotium), fixed and permeabilized for endogenous RASA2 detection using polyclonal rabbit anti-RASA2 antibody (Novus Biologicals) and Alexa Fluor 488-conjugated goat anti-rabbit IgG, and DAPI-stained. RAS activation at the Golgi upon TCR stimulation was examined similarly as in (36).  $G_{\alpha i2}$  KO Jurkat T cells were transfected with plasmids expressing mCherry-RBD, Cerulean-GalT, EGFP-HRAS/ NRAS, and  $G_{\alpha i2}$ . Transfected cells were plated on non-treated or anti-CD3-coated chambered coverglasses. After 5 min, single cells expressing all fluorescent proteins in the field of view were imaged. Confocal images were acquired on either Airyscan-equipped LSM800 confocal (Zeiss) or SP8 confocal (Leica) microscopes. Images were taken with fixed acquisition settings, then analyzed and automated using customized macro programs within ImageJ software. For fluorescence lifetime imaging microscopy (FLIM), 293T cells transfected with plasmids expressing mTFP1 and YFP were fixed and imaged on a Leica DMI 6000 SP5 confocal microscope. mTFP1 was excited at 805 nm with a femtosecond mode-locked (80 MHz repetition rate) Mai-Tai HP pulsed, multi-photon laser (Spectra Physics). Fluorescence was passed through a band-pass GFP filter at ET 525/50 (Chroma Technology Corp) and collected using a HPM100 Hybrid Detector R3809U-50 (Becker & Hickl: Hamamatsu Photonics). With SPC830 acquisition board, fluorescence decays were resolved by time-correlated single-photon counting. Acquired fluorescent transients were analyzed using SPCImage software according to single-life time decay and in ImageJ to determine FRET efficiencies in region of interest (ROI).

#### REFERENCES AND NOTES

- A. G. Gilman, G proteins: Transducers of receptor-generated signals. Annu. Rev. Biochem. 56, 615–649 (1987). doi: 10.1146/ annurev.bi.56.070187.003151; pmid: 3113327
- N. Wettschureck, S. Offermanns, Mammalian G proteins and their cell type specific functions. *Physiol. Rev.* 85, 1159–1204 (2005). doi: 10.1152/physrev.00003.2005; pmid: 16183910
- W. M. Oldham, H. E. Hamm, Structural basis of function in heterotrimeric G proteins. Q. Rev. Biophys. 39, 117–166 (2006). doi: 10.1017/S0033583506004306; pmid: 16923326
- V. Syrovatkina, K. O. Alegre, R. Dey, X. Y. Huang, Regulation, Signaling, and Physiological Functions of G-Proteins. J. Mol. Biol. 428, 3850–3868 (2016). doi: 10.1016/j.jmb.2016.08.002; pmid: 27515397
- R. Taussig, J. A. Iñiguez-Lluhi, A. G. Gilman, Inhibition of adenylyl cyclase by Gi alpha. Science 261, 218–221 (1993). doi: 10.1126/science.8327893; pmid: 8327893
- R. K. Sunahara, R. Taussig, Isoforms of mammalian adenylyl cyclase: Multiplicities of signaling. *Mol. Interv.* 2, 168–184 (2002). doi: 10.1124/mi.2.3.168; pmid: 14993377
- R. Sadana, C. W. Dessauer, Physiological roles for G proteinregulated adenylyl cyclase isoforms: Insights from knockout and overexpression studies. Neurosignals 17, 5–22 (2009). doi: 10.1159/000166277; pmid: 18948702
- 8. G. P. Solis *et al.*, Pediatric Encephalopathy: Clinical, Biochemical and Cellular Insights into the Role of Gln52 of

- GNA01 and GNAI1 for the Dominant Disease. Cells 10, 2749 (2021). doi: 10.3390/cells10102749; pmid: 34685729
- A. Marivin et al., Dominant-negative Gα subunits are a mechanism of dysregulated heterotrimeric G protein signaling in human disease. Sci. Signal. 9, ra37 (2016). doi: 10.1126/ scisignal.aad2429; pmid: 27072656
- L. S. Weinstein, M. Chen, T. Xie, J. Liu, Genetic diseases associated with heterotrimeric G proteins. *Trends Pharmacol.* Sci. 27, 260–266 (2006). doi: 10.1016/j.tips.2006.03.005; pmid: 16600389
- X. Huang et al., Pleiotropic phenotype of a genomic knock-in of an RGS-insensitive G184S Gnai2 allele. Mol. Cell. Biol. 26, 6870–6879 (2006). doi: 10.1128/MCB.00314-06; pmid: 16943428
- U. Rudolph et al., Ulcerative colitis and adenocarcinoma of the colon in G alpha i2-deficient mice. Nat. Genet. 10, 143–150 (1995). doi: 10.1038/ng0695-143; pmid: 7663509
- J. Lyons et al., Two G protein oncogenes in human endocrine tumors. Science 249, 655–659 (1990). doi: 10.1126/ science.2116665; pmid: 2116665
- F. Lecoquierre et al., Variant recurrence in neurodevelopmental disorders: The use of publicly available genomic data identifies clinically relevant pathogenic missense variants. Genet. Med. 21, 2504–2511 (2019). doi: 10.1038/s41436-019-0518-x; pmid: 31036916
- N. Hamada et al., Role of a heterotrimeric G-protein, Gi2, in the corticogenesis: Possible involvement in periventricular nodular heterotopia and intellectual disability. J. Neurochem. 140, 82–95 (2017). doi: 10.1111/jnc.13878; pmid: 27787898
- E. M. Scott et al., Characterization of Greater Middle Eastern genetic variation for enhanced disease gene discovery.
   Nat. Genet. 48, 1071–1076 (2016). doi: 10.1038/ng.3592; pmid: 27428751
- K. J. Karczewski et al., The mutational constraint spectrum quantified from variation in 141,456 humans. Nature 581, 434–443 (2020). doi: 10.1038/s41586-020-2308-7; pmid: 32461654
- S. R. Sprang, Invited review: Activation of G proteins by GTP and the mechanism of Gα-catalyzed GTP hydrolysis. *Biopolymers* 105, 449–462 (2016). doi: 10.1002/bip.22836; pmid: 26996924
- D. M. Berman, T. M. Wilkie, A. G. Gilman, GAIP and RGS4 are GTPase-activating proteins for the Gi subfamily of G protein alpha subunits. Cell 86, 445–452 (1996). doi: 10.1016/ S0092-8674(00)80117-8: pmid: 8756726
- K. L. Lan et al., A point mutation in Galphao and Galphail blocks interaction with regulator of G protein signaling proteins. J. Biol. Chem. 273, 12794–12797 (1998). doi: 10.1074/jbc.273.21.12794; pmid: 9582306
- K. M. Knight et al., A universal allosteric mechanism for G protein activation. Mol. Cell 81, 1384–1396.e6 (2021). doi: 10.1016/j.molcel.2021.02.002; pmid: 33636126
- E. R. Neptune, H. R. Bourne, Receptors induce chemotaxis by releasing the betagamma subunit of Gi, not by activating Gq or Gs. Proc. Natl. Acad. Sci. U.S.A. 94, 14489–14494 (1997). doi: 10.1073/pnas.94.26.14489; pmid: 9405640
- M. J. Lorenowicz, M. Fernandez-Borja, P. L. Hordijk, cAMP signaling in leukocyte transendothelial migration. *Arterioscler. Thromb. Vasc. Biol.* 27, 1014–1022 (2007). doi: 10.1161/ ATVBAHA.106.132282; pmid: 17347487
- R. Hidi et al., Phosphodiesterase and cyclic adenosine monophosphate-dependent inhibition of T-lymphocyte chemotaxis. Eur. Respir. J. 15, 342–349 (2000). doi: 10.1034/ j.1399-3003.2000.15b21.x; pmid: 10706503
- L. Harvath, J. D. Robbins, A. A. Russell, K. B. Seamon, cAMP and human neutrophil chemotaxis. Elevation of cAMP differentially affects chemotactic responsiveness. *J. Immunol.* 146, 224–232 (1991). doi: 10.4049/jimmunol.146.1.224; pmid: 1701793
- J. E. Jun, I. Rubio, J. P. Roose, Regulation of ras exchange factors and cellular localization of ras activation by lipid messengers in T cells. Front. Immunol. 4, 239 (2013). doi: 10.3389/fimmu.2013.00239; pmid: 24027568
- D. R. Myers, B. Wheeler, J. P. Roose, mTOR and other effector kinase signals that impact T cell function and activity. *Immunol. Rev.* 291, 134–153 (2019). doi: 10.1111/imr.12796; pmid: 31402496
- Q. Riller, F. Rieux-Laucat, RASopathies: From germline mutations to somatic and multigenic diseases. *Biomed. J.* 44, 422–432 (2021). doi: 10.1016/j.bj.2021.06.004; pmid: 34175492
- H. Abrahamsen et al., TCR- and CD28-mediated recruitment of phosphodiesterase 4 to lipid rafts potentiates TCR signaling. J. Immunol. 173, 8487-4858 (2004). doi: 10.4049/ iimmunol.173.8.4847: pmid: 15470025

- R. Mosenden, K. Taskén, Cyclic AMP-mediated immune regulation—Overview of mechanisms of action in T cells. Cell. Signal. 23, 1009–1016 (2011). doi: 10.1016/ j.cellsig.2010.11.018; pmid: 21130867
- V. L. Wehbi, K. Taskén, Molecular Mechanisms for cAMP-Mediated Immunoregulation in T cells - Role of Anchored Protein Kinase A Signaling Units. Front. Immunol. 7, 222 (2016). doi: 10.3389/fimmu.2016.00222; pmid: 27375620
- M. C. Mendoza, E. E. Er, J. Blenis, The Ras-ERK and PI3K-mTOR pathways: Cross-talk and compensation. *Trends Biochem. Sci.* 36, 320–328 (2011). doi: 10.1016/j.tibs.2011.03.006; pmid: 21531565
- P. D. King, B. A. Lubeck, P. E. Lapinski, Nonredundant functions for Ras GTPase-activating proteins in tissue homeostasis. Sci. Signal. 6, rel (2013). doi: 10.1126/ scisignal.2003669; pmid: 23443682
- D. K. Simanshu, D. V. Nissley, F. McCormick, RAS Proteins and Their Regulators in Human Disease. *Cell* 170, 17–33 (2017). doi: 10.1016/j.cell.2017.06.009; pmid: 28666118
- N. Wlodarchak, Y. Xing, PP2A as a master regulator of the cell cycle. Crit. Rev. Biochem. Mol. Biol. 51, 162–184 (2016). doi: 10.3109/10409238.2016.1143913; pmid: 26906453
- T. G. Bivona et al., Phospholipase Cgamma activates Ras on the Golgi apparatus by means of RasGRP1. Nature 424, 694–698 (2003). doi: 10.1038/nature01806; pmid: 12845332
- 37. B. D. Manning, A. Toker, AKT/PKB Signaling: Navigating the Network. *Cell* **169**, 381–405 (2017). doi: 10.1016/j.cell.2017.04.001; pmid: 28431241
- A. M. Spiegel, L. S. Weinstein, Inherited diseases involving g proteins and g protein-coupled receptors. *Annu. Rev. Med.* 55, 27–39 (2004). doi: 10.1146/annurev.med.55.091902.103843; pmid: 14746508
- M. O'Hayre et al., The emerging mutational landscape of G proteins and G-protein-coupled receptors in cancer. Nat. Rev. Cancer 13, 412–424 (2013). doi: 10.1038/nrc3521; pmid: 23640210
- K. M. Nishiguchi et al., Defects in RGS9 or its anchor protein R9AP in patients with slow photoreceptor deactivation. Nature 427, 75–78 (2004). doi: 10.1038/nature02170; pmid: 14702087
- M. K. Ho, L. Y. Yung, Y. H. Wong, Disruption of receptor-mediated activation of G protein by mutating a conserved arginine residue in the switch II region of the alpha subunit.
   J. Neurochem. 73, 2101–2109 (1999). doi: 10.1046/j.1471-4159.1999.02101.x; pmid: 10537070
- D. M. Apanovitch, T. Iiri, T. Karasawa, H. R. Bourne, H. G. Dohlman, Second site suppressor mutations of a GTPase-deficient G-protein alpha-subunit. Selective inhibition of Gbeta gamma-mediated signaling. J. Biol. Chem. 273, 28597–28602 (1998). doi: 10.1074/ jbc.273.44.28597; pmid: 9786851
- T. Iiri, Z. Farfel, H. R. Bourne, Conditional activation defect of a human Gsalpha mutant. *Proc. Natl. Acad. Sci. U.S.A.* 94, 5656–5661 (1997). doi: 10.1073/pnas.94.11.5656; pmid: 9159128
- 44. B. S. Muntean et al., Gao is a major determinant of cAMP signaling in the pathophysiology of movement disorders. Cell Rep. 34, 108718 (2021). doi: 10.1016/j.celrep.2021.108718; pmid: 33535037
- A. Szabó, R. Mayor, Mechanisms of Neural Crest Migration. *Annu. Rev. Genet.* 52, 43–63 (2018). doi: 10.1146/ annurev-genet-120417-031559; pmid: 30476447
- R. J. Miller, G. Banisadr, B. J. Bhattacharyya, CXCR4 signaling in the regulation of stem cell migration and development. J. Neuroimmunol. 198, 31–38 (2008). doi: 10.1016/ j.jneuroim.2008.04.008; pmid: 18508132
- J. H. Kehrl, The impact of RGS and other G-protein regulatory proteins on Gαi-mediated signaling in immunity. *Biochem. Pharmacol.* 114, 40–52 (2016). doi: 10.1016/j.bcp.2016.04.005; pmid: 27071343
- K. Gollmer et al., CCL21 mediates CD4+ T-cell costimulation via a DOCK2/Rac-dependent pathway. Blood 114, 580–588 (2009). doi: 10.1182/blood-2009-01-200923; pmid: 19451552
- R. Weinkove, P. George, N. Dasyam, A. D. McLellan, Selecting costimulatory domains for chimeric antigen receptors: Functional and clinical considerations. *Clin. Transl. Immunology* 8, e1049 (2019). doi: 10.1002/cti2.1049; pmid: 31110702
- E. Shifrut et al., Genome-wide CRISPR Screens in Primary Human T Cells Reveal Key Regulators of Immune Function. Cell 175, 1958–1971.e15 (2018). doi: 10.1016/j.cell.2018.10.024
- J. Carnevale et al., RASA2 ablation in T cells boosts antigen sensitivity and long-term function. Nature 609, 174–182 (2022), doi: 10.1038/s41586-022-05126-w; pmid: 36002574

- C. R. Surve, J. Y. To, S. Malik, M. Kim, A. V. Smrcka, Dynamic regulation of neutrophil polarity and migration by the heterotrimeric G protein subunits Gαi-GTP and Gβγ. Sci. Signal. 9, ra22 (2016). doi: 10.1126/scisignal.aad8163; pmid: 26905427
- M. Zenker, Clinical overview on RASopathies. *Am. J. Med. Genet. C. Semin. Med. Genet.* 190, 414–424 (2022).
   doi: 10.1002/ajmg.c.32015; pmid: 36428239
- Y. Aoki, T. Niihori, S. Inoue, Y. Matsubara, Recent advances in RASopathies. J. Hum. Genet. 61, 33–39 (2016). doi: 10.1038/ jhg.2015.114; pmid: 26446362
- C. R. Quaio et al., Autoimmune disease and multiple autoantibodies in 42 patients with RASopathies. Am. J. Med. Genet. A. 158A, 1077–1082 (2012). doi: 10.1002/ ajmg.a.35290; pmid: 22488759
- R. Árafeh et al., Recurrent inactivating RASA2 mutations in melanoma. Nat. Genet. 47, 1408–1410 (2015). doi: 10.1038/ ng.3427; pmid: 26502337
- F. Raimondi et al., Rare, functional, somatic variants in gene families linked to cancer genes: GPCR signaling as a paradigm. Oncogene 38, 6491–6506 (2019). doi: 10.1038/s41388-019-0895-2: pmid: 31337866
- M. Krauthammer et al., Exome sequencing identifies recurrent mutations in NF1 and RASopathy genes in sun-exposed melanomas. Nat. Genet. 47, 996–1002 (2015). doi: 10.1038/ ng.3361: pmid: 26214590
- N. Sobreira, F. Schiettecatte, D. Valle, A. Hamosh, GeneMatcher: A matching tool for connecting investigators with an interest in the same gene. *Hum. Mutat.* 36, 928–930 (2015). doi: 10.1002/humu.22844; pmid: 26220891
- J. T. den Dunnen et al., HGVS Recommendations for the Description of Sequence Variants: 2016 Update. Hum. Mutat. 37, 564–569 (2016). doi: 10.1002/humu.22981; pmid: 26931183
- D. Egger-Adam, V. L. Katanaev, The trimeric G protein Go inflicts a double impact on axin in the Wnt/frizzled signaling pathway. *Dev. Dyn.* 239, 168–183 (2010). doi: 10.1002/ dvdy.22060; pmid: 19705439
- C. Lin et al., Double suppression of the Gα protein activity by RGS proteins. Mol. Cell 53, 663–671 (2014). doi: 10.1016/ i.molcel.2014.01.014; pmid: 24560274
- M. Soto-Velasquez, M. P. Hayes, A. Alpsoy, E. C. Dykhuizen, V. J. Watts, A Novel CRISPR/Cas9-Based Cellular Model to Explore Adenylyl Cyclase and cAMP Signaling. *Mol. Pharmacol.* 94, 963–972 (2018). doi: 10.1124/mol.118.111849; pmid: 29950405
- I. T. Lamborn et al., Recurrent rhinovirus infections in a child with inherited MDA5 deficiency. J. Exp. Med. 214, 1949–1972 (2017). doi: 10.1084/jem.20161759; pmid: 28606988
- 65. H. J. Bailes, R. J. Lucas, Human melanopsin forms a pigment maximally sensitive to blue light (\(\lambda\) max ≈ 479 nm) supporting activation of G(q/11) and G(i/o) signalling cascades. Proc. R. Soc. Lond. Ser. B 280, 20122987 (2013). doi: 10.1098/ rspb.2012.2987; pmid: 23554393
- M. A. Gargano et al., The Human Phenotype Ontology in 2024: Phenotypes around the world. Nucleic Acids Res. 52, D1333–D1346 (2024). doi: 10.1093/nar/gkad1005; pmid: 37953324
- K. G. Anderson et al., Intravascular staining for discrimination of vascular and tissue leukocytes. Nat. Protoc. 9, 209–222 (2014). doi: 10.1038/nprot.2014.005; pmid: 24385150
- S. A. Cook et al., HEM1 deficiency disrupts mTORC2 and F-actin control in inherited immunodysregulatory disease. Science 369, 202–207 (2020). doi: 10.1126/science.aay5663; pmid: 32647003
- D. B. Kuhns, E. DeCarlo, D. M. Hawk, J. I. Gallin, Dynamics of the cellular and humoral components of the inflammatory response elicited in skin blisters in humans. *J. Clin. Invest.* 89, 1734–1740 (1992). doi: 10.1172/JC1115775; pmid: 1601984
- J. S. Bender, H. Thang, M. Glogauer, Novel rinse assay for the quantification of oral neutrophils and the monitoring of chronic periodontal disease. *J. Periodontal Res.* 41, 214–220 (2006). doi: 10.1111/j.1600-0765.2005.00861.x; pmid: 16677291
- A. Seki, S. Rutz, Optimized RNP transfection for highly efficient CRISPR/Cas9-mediated gene knockout in primary T cells. J. Exp. Med. 215, 985–997 (2018). doi: 10.1084/jem.20171626; pmid: 29436394
- E. K. Brinkman, T. Chen, M. Amendola, B. van Steensel, Easy quantitative assessment of genome editing by sequence trace decomposition. *Nucleic Acids Res.* 42, e168 (2014). doi: 10.1093/nar/gku/936; pmid: 25300484
- P. J. Boersema, R. Raijmakers, S. Lemeer, S. Mohammed,
   A. J. Heck, Multiplex peptide stable isotope dimethyl labeling

- for quantitative proteomics. *Nat. Protoc.* **4**, 484–494 (2009). doi: 10.1038/nprot.2009.21; pmid: 19300442
- J. Cox, M. Mann, MaxQuant enables high peptide identification rates, individualized p.p.b. range mass accuracies and proteome-wide protein quantification. *Nat. Biotechnol.* 26, 1367–1372 (2008). doi: 10.1038/nbt.1511; pmid: 19029910
- Y. Perez-Riverol et al., The PRIDE database resources in 2022: A hub for mass spectrometry-based proteomics evidences. Nucleic Acids Res. 50, D543–D552 (2022). doi: 10.1093/nar/gkal1038; pmid: 34723319
- T. F. Brust, J. M. Conley, V. J. Watts, Gα(i/o)-coupled receptormediated sensitization of adenylyl cyclase: 40 years later.
   Eur. J. Pharmacol. 763, 223–232 (2015). doi: 10.1016/ j.ejphar.2015.05.014; pmid: 25981304
- I. T. Lamborn, "The genetic, molecular, and cellular bases of unidentified primary immunodeficiencies," thesis, University of Pennsylvania (2016).
- M. D. Mailman et al., The NCBI dbGaP database of genotypes and phenotypes. Nat. Genet. 39, 1181–1186 (2007). doi: 10.1038/ng1007-1181; pmid: 17898773

A portion of this work was previously included in I.T.L.'s Ph.D.

#### **ACKNOWLEDGMENTS**

thesis dissertation at the University of Pennsylvania as part of the NIH MD/PhD partnership program (77). The authors thank the patients and family members for participating in this study and making this research possible. We thank J. McElwee, C. Gonzaga-Jauregui, J. Niemela. M. Menezes, and A. Lermine for sequencing and bioinformatics assistance; E. Masutani, H. Murdock, M. Leney-Greene, J. Qin, and V. Vignard for other technical assistance; M. Abaandou, P. Angelus, A. Wang, T. Dimaggio, and D. McDermott for regulatory assistance; P. Quackenbush for performing skin punch biopsies; D. Hilligoss for suction blister induction: J. Hammer, C. Happel. J. Katz, K. Keppler-Noreuil, C. Koh, S. Ardoin, R. Olshefski, D. Macdonald, D. Fitzgerald, G. Ambler, M. Stormon, C. Troedson, N. Armitage, A. Morrow, A. Agharahimi, C. Muraresku, V. Baghin, S. Prader, A. Gerard, L. Satter, M. Hempel, and G. Weinberg for clinical care; G. Morel, K. Hannula-Jouppi, and J. Kere for diagnostic studies; and P. Schwartzberg, S. Tangye, J. Kehrl, O. Schwartz, K. Hedin, and V. Shapiro for helpful discussions. Some figures were created with BioRender.com. Funding: This work was supported by the NIH, Department of Health and Human Services, through the Intramural Research Programs of the National Institute of Allergy and Infectious Diseases (NIAID) (1ZIAAI001059 to H.C.S.; 1Z01AI000717 to M.J.L.; 1Z01AI000758 to R.N.G.; ZIAAI000939 to K.M.D.; 17IAAI001156 to T I: 7IAA1001247 to A F F: and 17ICAI001244): the National Human Genome Research Institute (NHGRI) (1ZIAHG200407 to C.R.F); the National Heart, Lung, and Blood Institute (NHLBI) (1ZIAHL006200 to K.N.O.); the National Institute of Dental and Craniofacial Research (NIDCR) (1ZIADE000732 to N.M.); the National Institute of Child Health and Human Development (NICHD) (17IAHD008920 to C.A.S.): the National Institute of Arthritis and Musculoskeletal and Skin Diseases (NIAMS) (1ZIAARO41219 to H.H.K.); and the National Institute of Diabetes and Digestive and Kidney Diseases (NIDDK) (1ZICDK062009 to D.E.A.); and in part with federal funds from the NIAID under Bioinformatics and Computational Biosciences Branch (BCBB) Support Services Contract HHSN316201300006W/75N93022F00001 to Guidehouse and to the National Cancer Institute (NCI) under contract nos. 75N91019D00024 and HHSN261200800001E. It utilized the Genomic Research Integration System (GRIS) and highperformance computational capabilities of the OCICB High Performance Computing cluster at NIAID, Bethesda, MD. Molecular graphics and analyses were performed with UCSF Chimera, developed by the Resource for Biocomputing, Visualization, and Informatics at the University of California, San Francisco, with support from NIH P41-GM103311. H.H. was supported by a grant from the Korea Research Institute of Bioscience and Biotechnology (KRIBB) Research Initiative Program (Korean Biomedical Scientist Fellowship Program), Republic of Korea, I.T.L was a Medical Scientist Training Program student in the graduate program in immunology at the University of Pennsylvania. Support was also provided by Fonds de la Recherche en Santé du Québec, Canada (to Y.A.B.); Intramural Funding of the ZMNH (to M.K.); Japan Society for the Promotion of Science and Mochida Memorial Foundation for Medical and Pharmaceutical Research (to K.M.); the French network of University Hospitals HUGO (Hôpitaux Universitaires du Grand Ouest), and the French Ministry of Health and the Health Regional Agencies from Poitou-Charentes, Bretagne, Pays de la Loire, and Centre-Val de Loire (HUGODIMS, 2013, RC14\_0107) (to B.I., S.Bé.); the Swiss National Science Foundation (project no. 320030\_205097) (to J.P.S.); the Foundation for Pediatric Research, Finland (to M.M.): the Howard Hughes Medical Institute, the Rockefeller University, the St. Giles Foundation, the

Sciences (NCATS), NIH Clinical and Translational Science Award (CTSA) program (UL1 TR001866), the French National Research Agency (ANR) under the Investments for the Future program (ANR-10-IAHU-01), the Integrative Biology of Emerging Infectious Diseases Laboratory of Excellence (ANR-10-LABX-62-IBEID), LTh-MSMD-CMCD (ANR-18-CE93-0008-01), the French Foundation for Medical Research (FRM) (EQU201903007798), the Square Foundation, Grandir Fonds de solidarité pour l'enfance, the SCOR Corporate Foundation for Science, William E. Ford, General Atlantic's Chairman and Chief Executive Officer, Gabriel Caillaux, General Atlantic's Co-President, Managing Director and Head of Business in EMEA and the General Atlantic Foundation, the Battersea & Bowery Advisory Group, Institut National de la Santé et de la Recherche Médicale (INSERM), and the University of Paris Cité (to A.P. and J.L.C.): the Wallace Family Research Fund (to Ja.Ch.); the Care-for-Rare Foundation (C4R, 160073), the Else Kröner-Fresenius Stiftung (EKFS, 2017\_A110), the German Federal Ministry of Education and Research (BMBF 01GM2206D) (to F.H): the Hertie Foundation (P1230037 to M.Wa.): the National Health and Medical Research Council (APP1081858 to E.M., APP1113904 to R.B., and APP1108800 to C.C.G.); the Bill and Patricia Ritchie Foundation (to E.M. and C.C.G.): the Richard and Anne Borch Research Award, Purdue University (to V.J.W.); NIAID R01 Al120949 and the Mayo Clinic Foundation (to D.D.B.); USPHS grant AI-139633 and the Perkin Foundation (to R.S.G.); the Sigrid Jusélius Foundation, Finland (to O.M.M.); The Royal Children's Hospital Foundation through the Chair in Genomic Medicine (to Jo.Ch.): the Danica Foundation (to T.P.S.): and the Swiss National Science Foundation grant 31003A\_175658 (to V.L.K.). Research conducted at the Murdoch Children's Research Institute was supported by the Victorian Government's Operational Infrastructure Support Program. WES of P1 was performed in kind by Merck. The research was made possible in part through access to data generated by the France Genomic Medicine 2025 Plan. The content of this publication does not necessarily reflect the views or policies of the Department of Health and Human Services, nor does the mention of trade names, commercial products, or organizations imply endorsement by the US Government. Author contributions: H.H. identified the interaction between active G., and RASA2, performed experiments examining TCR-induced responsiveness of mutant  $G_{\alpha i2}$ -transduced T cells, TCR-induced signaling of patient T cells, transduced T cells, and RASA2-depleted T cells; validated GNAI2 mutant allele (P1)-specific KOs; and performed GST pulldowns, coimmunoprecipitations, GAP assays, confocal microscopy, FLIM imaging, in vitro chemotaxis, and GTPase assays, H.J. performed experiments evaluating  $\textbf{G}_{\alpha i2}$  variants by cAMP ELISA or reporter BRET assay and in vitro transwell chemotaxis, TCR-induced responsiveness of patient and KO T cells [GNAI2 mutant allele (P1), RASA2, and ACs], and TCR-induced signaling of AC-KO T cells. I.T.L. identified and established the causal nature of patient GNAI2 mutations; made initial observation of impaired chemotaxis, Ca2+ flux, and TCR-induced hyperresponsiveness; and performed experiments examining proximal and downstream signaling, in vitro transwell chemotaxis, chemokine-induced  $\text{Ca}^{2+}$  flux, and  $G_{\alpha i2}$  expression in patient and mutant  $G_{\alpha i2}$ -transduced T cells. I.T.L., J.N.M., and R.N.G. studied chemotaxis in vivo by using adoptive cell transfer. M.M.K. performed TCR-induced activation and signaling experiments of patient T cells. A.K. and V.L.K. performed GTP binding and GTP hydrolysis by Gai variants and analyzed data, Y.A.B. and T.P.S. set up BRET assay to evaluate mutant  $G_{\alpha i2}$  from P1 and examine the interaction of  $G_{\alpha i2}$ and GPCR. D.E.A. performed mass spectrometry analysis to identify interacting proteins. K.M.D. performed RGS protein pulldown. M.K. and S.R. performed cAMP measurements of  $G_{\alpha i2}$  variants with Glosensor. D.B.K., D.L.F., X.X, W.S.K., and T.J. performed EZ-TAXIScan experiments. K.A.Z. evaluated leukocyte migration into blisters. N.M.M. evaluated cell accumulation in oral mucosa. H.H.K. performed skin virome analysis. P.C. performed molecular modeling. M.M.K. J.D., and D.T. assisted in G<sub>αi2</sub> expression, in vitro chemotaxis, GTPase assays, and processing patient samples. K.Me. performed coimmunoprecipitation of exogenously expressed RASA2 with  $G_{\alpha i2}$ variants. M.F.R.Q. assisted with TCR-induced signaling experiments of patient T cells. S.G. and J.K. assisted with imaging capture and analyses. E.M.-F., R.B., and C.C.G. generated and evaluated the Gnai2 KI mice. V.J.W. generated the AC3 and AC6 double KO HEK293 cells and advised on cAMP assays. D.D.B. assisted in analyses of data for manuscript preparation. Experimental patient biospecimens and clinical data were collected/curated by P.J.M., H.C.S., J.T., B.I., A.F.F., Z.Z.-C., C.K., L.F., P.E., W.A.-H., J.P.S., K.V., P.A.T., V.B., L.P., M.M., P.L., K.N.O., A.N., M.L.-N., B.M., O.M.M., F.H., P.S., M.Wo., K.E.S., M.SI., M.So., H.H.K., S.Ba., H.S., R.J., and D.L. Genetic studies (WES, WGS, Ion Torrent panel, and Sanger confirmation) were performed, analyzed, or coordinated by Y.Z., S.K., C.S., R.J.T., N.C., C.K., F.L., M.Wa., R.P., M.M., A.P.,

NIH (R01Al127564), the National Center for Advancing Translational

J.Cho., G.L., A.-L.B., M.T., P.L., T.B., J.D., G.T., Y.D., A.P.H., J.S., S.L., M.Si., J.-L.C., O.M.M, J.Chr., S.Bé., R.S.G., C.A.S., H.S., B.K., B.B.-P., P.B., and K.Mc. Across the patient cohort, dysmorphism and skeletal imaging were evaluated and analyzed by C.R.F., neurological imaging was analyzed by A.S., and histopathologic analyses were performed by S.P. A.F.F. and I.T.L. assisted H.C.S. in overall clinical data curation. A.J.O. performed categorical analyses of HPO data. J.G. assisted with statistical analyses. H.F.M. coordinated clinical study protocol and sample collection, H.C.S. planned and supervised the experimental work and data analyses. M.J.L. provided advice and assisted in supervising experimental work. Y.Z. performed, supervised, and coordinated genetic studies including Sanger sequencing mutation confirmations, WES reanalysis across the cohort, and RNA-seg analyses. H.H., H.J., I.T.L., M.J.L., and H.C.S. prepared the manuscript. All authors read and discussed the submitted manuscript. Competing interests: H.C.S. holds stock in Amgen and Eli Lilly. K.M. is an employee of GeneDx, a genetic testing laboratory. R.J.T. is an Illumina employee and shareholder. J.P.S. was a member of a data monitoring committee for leniolisib for SOBI and Pharming within the last 3 years. C.A.S. was a paid consultant for Lundbeck pharmaceuticals, C.A.S. is an inventor on patent applications US-20030022180-A1 held by NIH that covers PRKAR1A and Carney complex, US-20090005337-A1

held by NIH that covers PDE11A and adrenal disease, and US-20170304405-A1 held by NIH that covers treatment of hormonal disorders of growth C.A.S. and G.T. are inventors on patent application US-20190314459-A1 held by NIH that covers GPR101 function. The other authors declare that they have no competing interests. Data and materials availability: All data needed to evaluate the conclusions in the paper are present in the paper or the supplementary materials. The WES datasets, where permitted under terms of patient informed consent for patients 1 to 6, 8 to 14. and 18, were deposited to the National Center for Biotechnology Information's database of Genotypes and Phenotypes (dbGaP) (78) (accession number phs002817.v1.p1) under controlled access for qualified investigators and their institutions in accordance with potentially sensitive patient information. WES datasets for patients P7 and P15 are available to qualified investigators through Internetiational data transfer agreements, requests should be made through the corresponding author. Wis datasets for Many and Elis Jk. Mis. as an employee of demands, and the collecters Analyses of Bondes and Planting within the last 3 years. CAS. as a paid consistent for Lundezo pharmacolitics. CAS. since a paid consistent for Lundezo pharmacolitics. CAS is an amount of the committee (CSF)-validated research projects. P12 and P14 familial matches we deposited in the (CNF) where Consistent of Elisis Committee (CSF)-validated research projects. P12 and P14 familial matches we deposited in the (CNF) where Consistent of Elisis Committee (CSF)-validated research projects. P12 and P14 familial matches we deposited the for Uniforthy dedubes on the Circles and P14 familial matches we deposited the Circles and P14 familial matches we deposited the Circles and P14 familial matches and P14 familial matches we deposited the Circles and P14 familial matches and P14 fa interinstitutional data transfer agreements; requests should be made through the corresponding author. WGS datasets for P17 and P20 will be deposited to the Collecteur Analyseur de Données

Consortium through the PRIDE (75) partner repository with the dataset identifiers PXD048980 and 10.6019/PXD048980. Patient samples are available from H.C.S. through a material transfer agreement for human materials from the NIH. License information: Copyright @ 2024 the authors, some rights reserved; exclusive licensee American Association for the Advancement of Science. No claim to original US government works. https://www. science.org/about/science-licenses-journal-article-reuse

#### SUPPLEMENTARY MATERIALS

science.org/doi/10.1126/science.add8947 Materials and Methods Supplementary Text Figs. S1 to S27 Tables S1 to S9 References (79-100) Movies S1 to S3